Hydraulic architecture explains species moisture dependency but not mortality rates across a tropical rainfall gradient

Alexandria L. Pivovaroff[1*], Brett T. Wolfe[2,3], Nate McDowell[1], Bradley Christoffersen[4], Stuart Davies[2], L. Turin Dickman[5], Charlotte Grossiord[6,7], Riley T. Leff[1], Alistair Rogers[8], Shawn P. Serbin[8], S. Joseph Wright[2], Jin Wu[8,9], Chonggang Xu[5], Jeffrey Q. Chambers[10]

Affiliations

[1]Atmospheric Science and Global Change Division, Pacific Northwest National Laboratory, Richland WA 99354 USA

[2]Smithsonian Tropical Research Institute, Balboa, Republic of Panama

[3]School of Renewable Natural Resources, Louisiana State University, Baton Rouge, LA, U.S.A.

[4]University of Texas Rio Grande Valley, Department of Biology, Brownsville TX 78520 USA

[5]Los Alamos National Laboratory, Earth and Environmental Sciences Division, Los Alamos, NM 87545 USA

[6]Functional Plant Ecology, Community Ecology Unit, Swiss Federal Institute for Forest, Snow and Landscape Research (WSL), Lausanne, Switzerland

[7]Plant Ecology Research Laboratory - PERL, School of Architecture, Civil and Environmental Engineering ENAC, EPFL, Lausanne, Switzerland

[8]Brookhaven National Laboratory, Environmental and Climate Sciences, Upton NY 11973 USA

[9]School of Biological Sciences, The University of Hong Kong, Pokfulam Road, Hong Kong

[10]Lawrence Berkeley National Laboratory, Earth and Environmental Science Area, Berkeley, CA 94720 USA

*Corresponding author:
Email: alexandria.pivovaroff@pnnl.gov
Phone: +1 562 881 4640

Submission and Acceptance Dates:
Received: _____; Revised: _____(optional); Accepted: _____

ABSTRACT

Aim

Intensified droughts are affecting tropical forests across the globe. However, the underlying mechanisms of tree drought response and mortality are poorly understood. Hydraulic traits and especially hydraulic safety margins (HSMs), i.e. the extent to which plants buffer themselves from thresholds of water stress, provide insights into species-specific drought vulnerability.

Methods

We investigated hydraulic traits during an intense drought triggered by the 2015-2016 El Niño on 27 canopy trees across three tropical forest sites with differing precipitation. We capitalized on the drought event as a time when plant water status might approach or exceed thresholds of water stress. We investigated the degree to which these traits varied across the rainfall gradient, as well as relationships amongst hydraulic traits and species-specific optimal moisture and mortality rates.

Results

There were no differences among sites for any measured trait. There was strong coordination among traits, with a network analysis revealing two major groups of coordinated traits. In one group there were water potentials, turgor loss point, sapwood capacitance and density, HSMs, and mortality rate. In the second group there was leaf mass per area, leaf dry matter content, hydraulic architecture (leaf area to sapwood area ratio), and species-specific optimal moisture.

Conclusion

These results demonstrated that while species with greater safety from turgor loss had lower mortality rates, hydraulic architecture was the only trait that explained species' moisture

dependency. Species with a greater leaf area to sapwood area ratio were associated with drier sites and reduced their transpirational demand during the dry season via deciduousness.

KEYWORDS

Hydraulic safety margins, drought, tropical forest, El Niño, water potential, turgor loss point, leaf mass per area, sapwood capacitance

1. INTRODUCTION

Climate change, including intensified and more frequent drought (Trenberth *et al.*, 2014), is driving tree mortality and leading to forest degradation across the globe (Allen *et al.* 2015) and in many tropical forests (McDowell *et al.* 2018). Mortality rates vary widely among species (Condit *et al.* 1995, 2017, Brienen *et al.* 2015), suggesting a diversity of underlying physiological drought adaptation traits that can vary both within and across sites (Anderegg 2015). However, we do not yet have a complete picture of the processes and mechanisms underlying tree drought response and mortality**.** Understanding the mechanisms of tropical forest responses to drought has implications for tropical forest functioning and can help answer unresolved questions concerning the mechanisms of tree mortality (Hartmann *et al.* 2015).

Hydraulic traits and water relations play a crucial role in plant drought responses and act as key determinants of safety from hydraulic failure (Brodribb & Cochard 2009, Blackman *et al.* 2016). They regulate plant water use and influence a number of physiological processes. Hence, hydraulic traits can provide insights into how plants respond to abiotic stress (Meinzer & McCulloh 2013, Anderegg *et al.* 2016), including acute drought. Drought can limit soil moisture availability for plant transpiration and thus cause reductions in plant water status, i.e. water potential. As plants lose water, increased tension in the water column and declining water potential are coordinated with stomatal closure to slow desiccation (Martin-StPaul *et al.* 2017). However, plant dehydration does not completely stop with stomatal closure as water can still be lost via cuticular conductance (Kerstiens 1996, 2006). Continued water loss can lead to the depletion of stored water as well as the introduction of embolism in xylem conduits via cavitation. Embolized, or air-filled, xylem conduits cannot transport water, hence hydraulic conductance declines, and as more emboli occur plants can become subject to hydraulic failure

(Sperry & Love 2015). Some species have a suite of coordinated traits that support greater drought tolerance, while other species are highly susceptible to drought (Pivovaroff *et al.* 2016). For example, more negative turgor loss point, greater sapwood density, sapwood capacitance, and resistance to xylem cavitation can all contribute to drought adaptation.

One key metric of drought mortality risk is the hydraulic safety margin (Nardini *et al.* 2013, Anderegg *et al.* 2016). Hydraulic safety margins (HSMs) are the difference between thresholds of water stress and the minimum water status that a plant experiences (Ψ_{MIN}). Different thresholds of water stress include xylem vulnerability to cavitation (i.e. the water potential at 50% or 88% percent loss of hydraulic conductivity; Ψ_{50} and Ψ_{88} respectively), leaf wilting (i.e. the water potential at the turgor loss point; π_{TLP}), and the water potential at which sapwood capacitance is diminished (i.e. the water potential at the "elbow" of the cumulative water release curve, here called C_{ELBOW}, described in (Meinzer *et al.* 2009). The closer the water status of a plant comes to reaching its hydraulic threshold for water stress, the more likely the plant is to suffer hydraulic dysfunction. HSMs are potentially important traits in predicting tree death (Anderegg et al. 2016, but see (Wolfe 2017). While one might expect HSMs to be narrower at sites with lower mean annual precipitation, Choat *et al*. (2012) concluded that a majority of forest species operate within narrow HSMs ($\Psi_{MIN} - \Psi_{50}$), suggesting a convergence in vulnerability to drought across the planet regardless of mean annual precipitation (Choat *et al.* 2012). However, only 14 of the observed HSMs in that study were for tropical forest trees. Additionally, within a given site, HSMs can vary widely among species (Pivovaroff *et al.* 2018). Understanding mortality risk and HSMs for tropical species is limited, and to our knowledge this has not been investigated for a wide selection of tropical tree species across sites with different long-term precipitation nor during an acute drought event.

Environmental conditions play a major role in the distribution and abundance of tropical tree species. For example, soil nutrient limitation and precipitation have long been recognized as key factors in shaping tropical forest plant communities (Baillie *et al.* 1987, Gentry 1988, Bongers *et al.* 1999). In fact, multiple studies have found species-specific drought sensitivity in particular governs species distribution across the rainfall gradient that spans the isthmus of Panama (Engelbrecht *et al.* 2007, Condit *et al.* 2013). For example, Engelbrect *et al*. (2007) analyzed 48 tropical tree and shrub species across 122 sites and found that soil water availability was a direct determinant of species distribution across local and regional scales. In addition, Condit *et al*. (2013) examined the responses of 550 tropical tree species across 72 sites in Panama to eight environmental factors, including dry-season intensity and soil fertility, and found that dry-season intensity and soil phosphorus were the strongest predictors of species occurrence. Using fitted coefficients from Condit *et al*. (2013) that relate species' probability of occurrence to dry-season intensity, one can calculate individual species optimal position across this same precipitation gradient, or species-specific optimal moisture. Higher optimal moisture values mean a species is more highly associated with wet sites and therefore is more moisture dependent. Understanding the correlations among species' moisture requirements, mortality rates, and hydraulic traits is critical to predict tropical forest responses to climate change.

The goal of this research was to examine how plant hydraulic traits vary among a diverse set of dominant tree species across a tropical rainfall gradient, and to relate these traits to species-specific optimal moisture and mortality rates. To this end, we measured water potentials to determine the minimum seasonal water potential and the difference between the minimum seasonal water potential and the maximum seasonal water potential; pressure-volume curves to determine turgor loss point; water release curves to determine sapwood capacitance, the water

potential at the "elbow" of the water release curve, sapwood density; and morphological leaf traits including leaf mass per area, leaf dry matter content, and leaf area to sapwood area ratio. From these traits, we also calculated two HSMs: $\Psi_{MIN} - \pi_{TLP}$ and $\Psi_{MIN} - C_{ELBOW}$. We conducted this research during an intense drought triggered by the 2015-2016 El Niño, capitalizing on this event as a time when plant water status might approach or exceed thresholds of water stress (i.e. small or possibly negative HSMs). We hypothesized that: 1) Hydraulic traits would vary across sites with different long-term mean annual precipitation following coordinated drought strategies, 2) Species' hydraulic traits would be coordinated with their moisture dependency (i.e. less moisture dependent species would be more drought-tolerant and have multiple metrics of drought safety as indicated by their suite of traits) and mortality rate, and 3) HSMs specifically would be highly coordinated with others traits in a hydraulic trait network.

2. METHODS

2.1 Study sites and species

This study was conducted at three lowland tropical forest sites on the isthmus of Panama with varying precipitation (Figure 1a and b). This region has a distinct wet season and dry season, with the majority of rainfall (>75%) occurring during the wet season (May – November). The first site, Parque Natural Metropolitano (PNM; 8°58′N, 79°34′W), is a seasonally dry forest with a mean annual precipitation of 1850 mm. The second site, Barro Colorado Island (BCI, 9°10′N, 79°51′W), is a lowland tropical moist forest with a mean annual precipitation of 2623 mm. The third site, Fort San Lorenzo (SLZ, 9°17′N, 79°58′W), is a wet evergreen forest with a mean annual precipitation of 3300 mm (Figure 1). Monthly precipitation summaries for each site were

downloaded from the Smithsonian Tropical Research Institute 'Physical Monitoring Program' site (http://biogeodb.stri.si.edu/physical_monitoring/research/).

Nine locally abundant canopy tree species (PNM *n*=9, BCI *n*=9, SLZ *n*=9) were selected at each site, for a total of 27 tree species (Table 1). Species were selected with the criteria of: (1) occurring within the footprint of the canopy crane for sample access (except at BCI, which has no canopy crane), (2) having leaves at the time of measurement, and (3) spanning a range of wood densities within each site (Table 1). Traits were measured on fully expanded, upper canopy sunlit leaves for one individual of each target species, except for pressure volume curves and water release curves, for which multiple individuals of each species were used. The PNM and SLZ sites have canopy access cranes that allowed sampling at the top of the forest canopy. However, BCI did not have a canopy access crane, and instead leaves were sampled from two telecommunication towers or by slingshot. Field campaigns to measure seasonal water potential occurred each month (February – May) of the dry season during the 2015 – 2016 El Niño event that was associated with anomalously low annual precipitation at each site, except at BCI where water potential measurements were limited to a single field campaign.

2.2 Leaf water potentials

Leaf water potential (Ψ; MPa) was measured on at least three leaves per tree for each study species during each field campaign using a Scholander-type pressure chamber to determine plant water status (PMS Instrument Co., Albany, OR, USA) over the course of the day, including predawn and midday. We defined the most negative water potential each species experienced over the course of the dry season as the minimum seasonal water potential (Ψ_{MIN}) (Bhaskar &

Ackerly 2006). In addition, $\Delta\Psi$ was defined as the difference between Ψ_{MIN} and the maximum water potential during our measurement period.

2.3 Leaf and stem traits

Following leaf water potential measurement, leaves were processed for additional traits. Leaf dry matter content (LDMC; g g^{-1}) and leaf mass per area (LMA; g m^{-2}) were measured by collecting a known leaf area using a cork borer, weighing it with a precision balance for fresh mass (Fisher Science Education, Model SNL303, Hanover Park, IL), then hydrating it for saturated mass, and finally drying it in an oven at 70°C for at least 48h until reaching a constant mass to determine dry mass. LDMC was determined as leaf dry mass (g) divided by saturated mass (g). LMA was determined as leaf dry mass (g) divided by fresh area (m^2).

From three to five terminal branches on each individual, cross-sectional sapwood area, leaf area to sapwood area (A_L:A_{SW}), and sapwood density (ρ_{SW}) were measured. Sapwood area (cm^2) was determined by removing bark from a 1-cm length of each sample and using digital calipers to measure sapwood diameter and pith diameter, and calculating the sapwood area minus the pith area. The total distal leaf area for each sample was measured with a leaf area meter (LI-3100C, LI-COR, Lincoln, NE, USA), to calculate A_L:A_{SW} (m^2 m^{-2}). ρ_{SW} was measured on fresh sapwood samples about 1cm in diameter, with the bark and pith removed. We used the water displacement method (Williamson & Wiemann 2010, Osazuwa-Peters *et al.* 2011) by attaching the sample to a needle and submerging the sample in a reservoir of water on a digital balance to determine the volume of water displaced by the sample, and then drying the samples in a drying oven at 70°C for at least 72h until reaching a constant mass to determine dry mass. ρ_{SW} was calculated as the ratio of dry mass (g) to fresh volume (cm^{-3}).

205

206 **2.4 Pressure-volume curves**

207 From the same target trees and others nearby, additional mature shoots with recently mature
208 leaves were collected to measure hydraulics traits including pressure-volume curves and
209 vulnerability curves (see below). Two to six pressure volume curves per species were measured
210 following (Koide *et al.* 1991), with the modification of determining leaf water potential on leaf
211 discs with a psychrometer (J.R.D. Merrill Specialty Equipment, Logan, Utah, USA). This
212 method has been shown to give results similar to those of the pressure chamber method (Nardini
213 *et al.* 2008). For each curve, a single leaf disc was progressively dried on the bench, with weight
214 and water potential measured at intervals to construct the pressure volume curves. Subsequently,
215 samples were placed in a drying oven at 70°C for at least 48h until reaching a constant mass to
216 determine dry mass. The typical time to complete a measurement for each leaf disc was 4-5
217 hours, with full curves taking multiple days. For each species, we measured a minimum of three
218 replicates. From the pressure-volume curves we calculated the water potential at turgor loss
219 (π_{TLP}; MPa). Raw pressure volume curves with fitted functions are provided in Supplemental
220 Figure 1, and box plots of TLP values for each curve by species are provided in Supplemental
221 Figure 2.

222

223 **2.5 Sapwood capacitance**

224 Sapwood capacitance was measured via water release curves (Tyree & Ewers 1991, Meinzer *et*
225 *al.* 2003). For each species, three branches were collected from the crowns of 2–3 trees. Upon
226 collection the branches were sealed in opaque plastic bags and transported to the laboratory.
227 Stem sections located 80-100cm from the apex were used for measurements. A sapwood sample

(i.e. secondary xylem, pith removed) 4cm in length was removed from each stem. While removing the samples, the stem sections were enveloped in moist paper towels to ensure that samples did not dry. The samples were weighed for fresh mass (m_F) and fresh volume (V_F) with water displacement on an analytical balance. Then they were submerged in distilled water for 24h and weighed for saturated mass (m_S) and saturated volume (V_S).

The samples were placed in pre-weighted custom-made nickel-coated aluminum chambers with inner dimensions of 25mm diameter and 45mm length. The chambers were connected to Peltier-type psychrometers (Merrill Instruments, Logan, UT) and placed in a water bath at 30°C for 3h to equilibrate the humidity within the chambers. Then water potential was measured using an automated multi-channel micro-voltmeter (CR7, Campbell Scientific, Logan, UT) with a 10s thermocouple cooling current. For samples with water potential < -4MPa, a 45s cooling current was used to improve accuracy. Each psychrometer probe was calibrated against salt solutions beforehand and the plateau of the psychromatic response curve was used to assess water potential.

After the initial measurement of water potential, the chambers were opened and the samples were allowed to air dry for periods of 0.5–2h. Then, mass and water potential were re-measured. This process was repeated until water potential reached < -7MPa. Dry mass was measured after drying the samples at 65°C for >72h.

At each point cumulative water released from the sample was calculated as:

$$Cumulative\ water\ release = \frac{m_S - m_F}{V_S}$$

Cumulative water release was plotted against water potential to construct the water release curves. Non-linear regression was used to fit a Gompertz function through each water release curve. The point at which the curve began to asymptote was taken as the point of maximum

change in slope (i.e., the point where the third derivative equaled zero, a.k.a the "elbow" of the cumulative water release curve; C_{ELBOW}; MPa) (Meinzer *et al.* 2009). Sapwood capacitance (C_{SW}; kg m^{-3} MPa^{-1}) was taken as the slope between this point and the origin. Raw cumulative water release curves with fitted functions are presented in Supplemental Figure 3.

2.6 Mortality rates

Species-specific instantaneous mortality rates were determined from the ForestGEO tree census data, which is publicly available through the ForestGEO Data Portal (http://ctfs.si.edu/datarequest/) (Condit 1998, Hubbell *et al.* 1999, Condit *et al.* 2009, 2019a, b). ForestGEO research plots are censused every 5 years, which involves identifying, tagging, and measuring all free-standing trees with a diameter at breast height (DBH) greater than 1cm. We calculated two mortality rates, the first using the 1995 and 2000 Barro Colorado Islanded censuses as these captured the 1997-1998 El Niño and hence mortality trends associated with moisture stress , and the 2010 and 2015 censuses, and these were the most recently available censuses. We used the 'mortality_ctfs()' function in the fgeo' package (ver. 1.1.4) to calculate species-specific instantaneous mortality rates as:

$$Z = \frac{\log(N) - \log(S)}{time}$$

where N is the number of individuals alive in the first census and S is the number of survivors (i.e. all individuals alive in both censuses). We filtered our mortality calculation to include only individuals with a minimum DBH of 20cm, as we measured traits on mature canopy trees and mortality rates can vary among size classes.

2.7 Species-specific optimal moisture

Condit *et al*. (2013) determined tree species composition for 72 sites across the same rainfall gradient and modeled species' occurrence as a function of eight environmental factors, including dry-season intensity. Dry season intensity was calculated as the cumulative moisture deficit D_{ij} between days i and j during the dry season as:

$$D_{ij} = \sum_{t=i}^{j} (P_t - E_t)$$

Where P_t was precipitation on day t and E_t was potential evapotranspiration on day t. When E_t exceeds P_t, as occurs during the dry season, D_{ij} takes negative values. The minimum D_{ij} for a year was their measure of dry season severity, and because the minimum D_{ij} is a negative value, the higher (or less negative) the value the moister it is. Condit *et al.* (2013) found that regional distributions were strongly affected by dry-season intensity for 57.6% of the 550 species present at 10 or more of their 72 sites. Using their fitted coefficients relating probability of occurrence to D_{ij} for each of our study species, we calculated each species optimal position across the central Panama rainfall gradient. More positive values indicate a species is associated with moister sites and more negative values indicate a species is associated with drier sites. We use this optimal position along the rainfall gradient as a proxy for species-specific optimal moisture, and the higher a species' optimal moisture, the more dependent it is on moisture.

2.8 Statistics

Two hydraulic safety margins (HSMs) were calculated relative to minimum seasonal water potential (Ψ_{MIN}), including (1) $\Psi_{MIN} - \pi_{TLP}$ and (2) $\Psi_{MIN} - C_{ELBOW}$. For HSMs, a more positive value indicates a safer strategy as the water status of the plant has not exceeded the

threshold measure, while a more negative value indicates a riskier strategy as the water status of the plant has exceeded the threshold measure.

Prior to analyses, variables were tested for normality using the Shapiro-Wilk test with the "stats" package (ver. 3.5.2). Variables that were not normally distributed were log transformed, except $\Psi_{MIN} - C_{ELBOW}$ because it had both positive and negative values.

We conducted an initial test for differences in measured traits (LMA, LDMC, A_L:A_{SW}, ρ_{SW}, C_{ELBOW}, C_{SW}, Ψ_{MIN}, π_{TLP}, $\Delta\Psi$, $\Psi_{MIN} - \pi_{TLP}$, $\Psi_{MIN} - C_{ELBOW}$, optimal moisture, and mortality rate) between leaf habit (evergreen or deciduous), but found no differences in traits between leaf habit except for ρ_{SW}. As this did not have a major impact on our results, we proceeded with testing for differences in measured traits among sites (hypothesis 1) using MANOVA with the "stats" package, as these represented multiple dependent variables for the independent variable of site, with each species serving as a replicate.

To test for coordination among species' hydraulic traits and with moisture dependency and mortality (hypothesis), we conducted an initial principal components analysis, presented in Supplemental Figure 4. Then we tested for correlations using Pearson correlation ($\alpha = 0.05$), with each species serving as a replicate, using the "rcorr" function in the "Hmisc" package (ver. 4.2). Using the results from the correlation matrix and following (Rosas *et al.* 2019), we characterized a hydraulic trait covariation network, with each trait treated as a node and each significant correlation treated as an edge that connected nodes (hypothesis 3). The nodes and edges were graphed with the "igraph" package (Csardi & Nepusz 2006). Two indicators of network centrality were calculated for each trait/node: 1) the degree of network centrality (D), defined as the number of edges for a node, and 2) the weighted degree of network centrality

(D_W), defined as the sum of the absolute values of all significant Pearson correlation coefficients for each node.

All statistics were done with R (ver. 3.5.2) (R Core Team 2020) in R Studio (ver. 1.1.463). Data associated with water potentials in this study are publicly available at the NGEE-Tropics dataset archive (Ely *et al.* 2019, Wolfe *et al.* 2019). Traits, their units, and corresponding symbol used in this manuscript are in Table 2.

3. RESULTS

There was no significant difference among sites for Ψ_{MIN}, $\Delta\Psi$, π_{TLP}, $\Psi_{MIN} - \pi_{TLP}$, C_{ELBOW}, $\Psi_{MIN} - C_{ELBOW}$ (Figure 2), A_L:A_{SW}, LMA, LDMC, ρ_{SW}, C_{SW}, (Figure 3), optimal moisture, or mortality (Figure 4) despite large differences in site-specific precipitation (Figure 1a).

There was coordination among traits (Figure 5), with LMA positively correlated with LDMC ($p = 0.0001$; $r = 0.68$) and negatively correlated with A_L:A_{SW} ($p = 0.03$; $r = -0.44$). ρ_{SW} was positively correlated with C_{ELBOW} ($p = 0.0500$; $r = 0.38$) and C_{SW} ($p = 0.0003$; $r = -0.64$). C_{SW} was also correlated with Ψ_{MIN} ($p = 0.01$; $r = 0.53$), $\Delta\Psi$ ($p = 0.02$; $r = 0.50$), $\Psi_{MIN} - \pi_{TLP}$ ($p = 0.02$; $r = 0.49$) and $\Psi_{MIN} - C_{ELBOW}$ ($p = 0.047$; $r = 0.42$); species with greater sapwood capacitance had less negative minimum seasonal water potential, a smaller change in water potential over the dry season, a greater or more positive $\Psi_{MIN} - \pi_{TLP}$ safety margin, and a greater or more positive $\Psi_{MIN} - C_{ELBOW}$ safety margin. Ψ_{MIN} was also positively correlated with $\Delta\Psi$ ($p < 0.0001$; $r = 0.95$), $\Psi_{MIN} - \pi_{TLP}$ ($p = 0.001$; $r = 0.72$) and $\Psi_{MIN} - C_{ELBOW}$ ($p = 0.01$; $r = 0.52$); species with a more negative minimum seasonal water potential had a greater change in water potential over the dry season, a smaller or more negative $\Psi_{MIN} - \pi_{TLP}$ safety margin, and a smaller or more negative $\Psi_{MIN} - C_{ELBOW}$ safety margin. In addition, $\Delta\Psi$ was positively

340 correlated with $\Psi_{MIN} - \pi_{TLP}$ ($p = 0.0005$; $r = 0.78$) and $\Psi_{MIN} - C_{ELBOW}$ ($p = 0.01$; $r = 0.52$);
341 species with a greater change in water potential over the dry season also had a smaller or more
342 negative $\Psi_{MIN} - \pi_{TLP}$ safety margin and $\Psi_{MIN} - C_{ELBOW}$ safety margin. $\Psi_{MIN} - \pi_{TLP}$ was
343 correlated with $\Psi_{MIN} - C_{ELBOW}$ ($p = 0.02$; $r = -0.48$) and π_{TLP} ($p = 0.02$; $r = 0.48$); species with a
344 greater or more positive $\Psi_{MIN} - \pi_{TLP}$ safety margin had a greater or more positive $\Psi_{MIN} - C_{ELBOW}$
345 safety margin, a more resistant or more negative turgor loss point. 2010-2015 mortality rates
346 were correlated with π_{TLP} ($p = 0.048$; $r = -0.5$) and $\Psi_{MIN} - \pi_{TLP}$ ($p = 0.02$; $r = -0.64$); species
347 with a greater or more positive $\Psi_{MIN} - \pi_{TLP}$ safety margin had a lower mortality rate. As the
348 1995-2000 mortality rates were also correlated with π_{TLP} ($p = 0.048$; $r = -0.51$) and $\Psi_{MIN} - \pi_{TLP}$
349 ($p = 0.03$; $r = -0.57$), we excluded them from further analysis (Supplemental figure 5). $\Psi_{MIN} -$
350 C_{ELBOW} and C_{ELBOW} were positively correlated ($p < 0.0001$; $r = 0.88$). The only trait that was
351 correlated with species-specific optimal moisture was A_L:A_{SW} ($p = 0.01$; $r = -0.48$), with more
352 moisture-dependent species having a lower A_L:A_{SW} and less moisture-dependent species having a
353 higher A_L:A_{SW} (Figure 6).

354 An analysis of network centrality for these measured traits (Figure 5) revealed that the
355 HSMs $\Psi_{MIN} - \pi_{TLP}$ was the most connected trait, with a degree of network centrality (*D)* equal to
356 6 (Table 2). C_{SW} and $\Psi_{MIN} - C_{ELBOW}$ were the next most connected traits, each with D equal to 5.
357 Furthermore, $\Psi_{MIN} - \pi_{TLP}$ also had the highest weighted degree of network centrality (D_W), with
358 $D_W = 3.58$ (Table 2), followed by $\Psi_{MIN} - C_{ELBOW}$ ($D_W = 2.81$), $\Delta\Psi$ ($D_W = 2.75$), Ψ_{MIN} ($D_W =$
359 2.7), and C_{SW} ($D_W = 2.56$).
360

361 **4. DISCUSSION**

We investigated plant hydraulic traits, including hydraulic safety margins (HSMs), during an intense drought triggered by the 2015-2016 El Niño event on 27 dominant canopy trees at three sites with differing historical precipitation across the isthmus of Panama. We capitalized on the drought event as a time when plant water status might approach or exceed thresholds of water stress, resulting in small or negative HSMs. We investigated how plant hydraulic traits vary among a diverse set of dominant tree species across a tropical rainfall gradient and related these traits to species-specific optimal moisture and mortality rates. We found there were no differences in any measured trait among sites (Figure 2, 3, and 4), opposing our first hypothesis that hydraulic traits would vary across sites with different long-term mean annual precipitation. We did find hydraulic trait coordination, with HSMs correlated with multiple other traits, supporting our second hypothesis (Figure 5). In addition, π_{TLP} and $\Psi_{MIN} - \pi_{TLP}$ were the only traits correlated with mortality rate (Figure 5). Finally, we found that A_L:A_{SW} was the only trait correlated with species-specific optimal moisture, with more moisture-dependent species (i.e. those with a higher optimal moisture value) having lower A_L:A_{SW} and less moisture-dependent species having higher A_L:A_{SW} (Figure 6).

Acute drought can be fatal for many plant species, as plants are sessile and unable to move to escape detrimental conditions. The probability of surviving is thought to be higher for species that typically operate well within a safe range of water potentials, i.e. have a larger HSM. Species that "live on the edge" and routinely experience water potentials close to levels of desiccation (i.e. have a smaller hydraulic safety margin) may be more likely to suffer drought mortality. Classically, HSMs are reported as the minimum water potential relative to xylem vulnerability to cavitation, specifically the water potential at 50% or 88% loss of conductivity (Ψ_{50} and Ψ_{88}, respectively). However, cavitation resistance is not the only threshold for water

stress. Other thresholds, including the water potential at stomatal closure, the turgor loss point, or significant depletion of sapwood capacitance, can be indicators of safety from hydraulic failure. When we compared species-specific mortality rates with two different HSMs, including $\Psi_{MIN} - \pi_{TLP}$ and $\Psi_{MIN} - C_{ELBOW}$, we found $\Psi_{MIN} - \pi_{TLP}$ was correlated (Figure 5); species with larger $\Psi_{MIN} - \pi_{TLP}$ safety margins had lower mortality rates, indicating that species whose water status exceeded their turgor loss point are more likely to die during drought. Turgor loss point is often used as a proxy for the water potential at stomatal closure, which occurs to avoid hydraulic failure in the vascular system (Bartlett *et al.* 2016, Martin-StPaul *et al.* 2017). In a seasonally dry tropical forest, (Powers *et al.* 2020) used a similar foliar hydraulic safety margin (the difference between the water potential at 50% of leaf embolism and the turgor loss point) rather than the "classic" stem Ψ_{50} or Ψ_{88}, and they found that species with a larger HSM were associated with lower mortality (Powers *et al.* 2020). This further supports the link between hydraulic traits and mortality (Anderegg *et al.* 2016), with hydraulic failure as a likely causal mechanism. We also found no differences in any HSM among sites, despite a wide sampling of canopy tree species as well as large historical differences in precipitation between sites. Previous studies have found similar trends. For example, two tropical forests with contrasting precipitation in the Amazon had similar hydraulic safety margins ($\Psi_{MIN} - \Psi_{50}$ and $\Psi_{MIN} - \Psi_{88}$) during the same 2015-2016 El Niño as our present study (Barros *et al.* 2019). In addition, at the same sites as our present study, while there were large differences in non-structural carbohydrates (NSC) among species, there were no seasonal differences in NSC as the drought progressed nor were there differences among sites (Dickman *et al.* 2019). Furthermore, an additional study found no differences in sap flux or sap flux sensitivity to VPD among these sites (Grossiord *et al.* 2019). One explanation could be that despite large variation in mean annual precipitation among sites, water is not a limiting

factor for this system. It is also possible that water is in fact limiting, and the degree of limitation is the same across sites. Another explanation is that HSMs are tightly constrained (Choat *et al.* 2012), even when using a water stress threshold besides Ψ_{50}.

It should be noted that a number of study species had negative HSMs, meaning the water status of the plant exceeded the defined thresholds of water stress. It is likely that the exceptional drought conditions present during the time of our study drove species beyond their typical range of plant water potentials, as was also seen in Tan *et al*. (2020) (Tan *et al.* 2020). This is supported by the evidence that multiple measures of HSM were negative (Figure 3). Furthermore, in the sequence of drought response traits, leaf wilting (π_{TLP}) occurs before 50% loss and 88% loss of stem hydraulic conductivity (Ψ_{50} and Ψ_{88}, respectively) (Bartlett *et al.* 2016), so negative HSMs based on Ψ_{MIN} - π_{TLP} would occur more frequently and be more common that stem vulnerability curve-based HSMs (such as Ψ_{MIN} - Ψ_{50} or Ψ_{MIN} – Ψ_{88}). Calculation of Ψ_{MIN} - Ψ_{50} using independent vulnerability curves measured using the pneumatic method (Pereira *et al.* 2016) for a subset of our species independently corroborate negative HSMs (Medina *unpublished data*; Smith-Martin *unpublished data*), though the pneumatic method is potentially subject to artifacts with long-vessel species (Sergent *et al.* 2020).

Our trait network analysis highlights the diversity of drought adaptation strategies present among moist tropical forest trees, with mechanistic implications for drought responses (Figure 5). Network analysis is often applied to social networks to identify the most influential person, or in epidemiology to identify disease super-spreaders. However, Rosas *et al*. (2019) recently applied network analysis to examine plant hydraulic trait relationships with water availability within species (Rosas *et al.* 2019). Here, we examined trait relationships among species and included HSMs. We found that traits grouped into two network paths. In the largest path, we

confirm classic trade-offs, such as between sapwood density and capacitance (Pratt *et al.* 2007, Scholz *et al.* 2007, McCulloh *et al.* 2014, Trifilò *et al.* 2015, Pratt & Jacobsen 2017, Savi *et al.* 2017, Santiago *et al.* 2018). In fact, we found that sapwood capacity and HSMs ($\Psi_{MIN} - \pi_{TLP}$ and $\Psi_{MIN} - C_{ELBOW}$) were among the most connected traits, having the highest degree of network centrality and among the top weighted degree of network centrality, which is explained by the integrative nature of these traits (Table 2). In addition, π_{TLP} and $\Psi_{MIN} - \pi_{TLP}$ were the only traits correlated with mortality rate. In the second path, we found that leaf functional traits grouped together, including LDMC, LMA, and A_L:A_{SW}. Furthermore, species-specific optimal moisture was a node in this path, and the only trait in our study that it was correlated with was A_L:A_{SW}; more moisture-dependent species (i.e. higher optimal moisture value) had lower A_L:A_{SW} and less moisture-dependent species (i.e. lower optimal moisture value) had higher A_L:A_{SW}. While some within-path relationships are explained by a commonality, such as Ψ_{MIN}, $\Delta\Psi$, and HSMs, and also leaf dry mass in LDMC and LMA, this does not negate the meaningful mechanisms underlying these relationships nor does it take away from the independence of the two network paths.

A_L:A_{SW}, the inverse of which is called the Huber value (Tyree & Ewers 1991), represents the total transpiring leaf area that must be supplied with water by the sapwood area, and is associated with pipe model theory (Shinozaki *et al.* 1964). Previous research has shown that hydraulic architecture plays a major role in regulating plant water use (Trugman, Anderegg, Sperry, *et al.* 2019, Trugman, Anderegg, Wolfe, *et al.* 2019) and is therefore a determinant of woody plant drought tolerance (Pivovaroff *et al.* 2016). Here, however, the relationship is at first surprising given that more moisture-dependent species in fact have a lower A_L:A_{SW}. One might assume that species associated with wetter sites would have the moisture availability to support a

larger transpiring leaf area. Here, however, leaf phenology is a key aspect to the relationship. While our *a priori* species selection criteria required study species to have leaves at the time of our field campaign during the dry season, this did not mean that all study species were in fact evergreen (Table 1). Deciduousness runs along a continuum, and we included a number of species that were obligate deciduous, facultative deciduous, and brevideciduous (leaf shed is followed by immediate flushing (Eamus & Prior 2001)). For these deciduous species, our field campaigns did not happen to align with the timing of their leaf shedding. We find that that more species have a deciduous leaf phenology at the driest site (eight out of nine study species are deciduous at PNM) versus the wettest site (three out of nine study species are deciduous at SLZ). These deciduous species only have to support a large leaf area for part of the year and can drop their leaves when conditions are less favorable, i.e. low moisture availability. Conversely, species found at moister sites having a lower A_L:A_{SW}, but they maintain this leaf area year-round. This is why five of the six species with an optimal moisture less than -1 are deciduous (Figure 6). This is further supported by evidence from seasonally dry tropical forests, which the follow the general relationship of evergreen species having smaller A_L:A_{SW} (or higher Huber values) and deciduous species have larger A_L:A_{SW} (or smaller Huber values) (Eamus & Prior 2001).

Understanding the physiological mechanisms that underlie tropical tree responses to intensified droughts helps us understand tree survival and mortality, which have implications for tropical forest dynamics and biogeochemical cycles (Cavaleri *et al.* 2017). Our finding that hydraulic architecture was the only trait that explained species' moisture dependency reveals that while HSMs are important traits for understandings species' drought tolerance and mortality risk (Anderegg *et al.* 2016), other traits warrant attention as well.

ACKNOWLEDGEMENTS

This work was supported by the Next-Generation Ecosystem Experiments (NGEE Tropics) projects that was supported by the Office of Biological and Environmental Research in the Department of Energy, Office of Science. AR and SPS were supported by the United States Department of Energy contract No. DE-SC0012704 to Brookhaven National Laboratory. CG was supported by the Swiss National Science Foundation SNF (PZ00P3_174068). BTW was supported by the National Institute of Food and Agriculture, U.S. Department of Agridulture, McIntire Stennis project uner LAB94493. The BCI forest dynamics research project was made possible by National Science Foundation (NSF) grants to Stephen P. Hubbell, with support from the Forest Global Earth Observatory, the Smithsonian Tropical Research Institute, the John D. and Catherine T. MacArthur Foundation, the Mellon Foundation, the Small World Institute Fund, and numerous private individuals, and through the hard work of over 100 people from 10 countries over the past three decades. The plot project is part the Forest Global Earth Observatory (ForestGEO), a global network of large-scale demographic tree plots. The CTFS R Package was developed with the support of NSF grant #1046113 to Stuart J. Davies through the NSF-IRCN program on the Dimensions of Biodiversity. Special thanks to Laura Fernandez De Una for translating our abstract to Spanish.

AUTHOR CONTRIBUTION STATEMENT

Alexandria L. Pivovaroff: Conceptualization, Formal analysis, Methodology, Visualization, Writing – original draft, Writing – review & editing

Nate McDowell: Conceptualization, Supervision, Writing – review & editing

Brett T. Wolfe: Investigation, Formal analysis, Data curation, Resources, Writing – review & editing

Bradley Christoffersen: Writing – review & editing

Stuart Davies: Data curation, Writing – review & editing

L. Turin Dickman: Writing – review & editing

Charlotte Grossiord: Writing – review & editing

Riley T. Leff: Software, Writing – review & editing

Alistair Rogers: Resources, Writing – review & editing

Shawn P. Serbin: Writing – review & editing

S. Joseph Wright: Methodology, Resources, Writing – review & editing

Jin Wu: Writing – review & editing

Chonggang Xu: Writing – review & editing

Jeffrey Q. Chambers: Funding acquisition, Supervision

CONFLICT OF INTEREST

No potential conflict of interest was reported by the authors.

Data availability statement

Meteorological data for these sites is publicly available from the Smithsonian Tropical Research Institute 'Physical Monitoring Program' site (http://biogeodb.stri.si.edu/physical_monitoring/research/).

ForestGEO census data for tree species at these sites, which was used to calculate species-specific mortality rates, is publicly available through the ForestGEO Data Portal (http://ctfs.si.edu/datarequest/).

Data related to the fitted coefficients relating probability of occurrence to dry season intensity for each of our study species, which were used to calculate species-specific optimal moisture, are available in the supplemental data for Condit et al. 2013.

Data related to water potentials in this study is available at the NGEE-Tropics dataset archive (Ely *et al.* 2019, Wolfe *et al.* 2019).

The raw pressure volume curves and stem water release curves are presented in the Supplemental Information (Supp. Figure 1 & 3, respectively). In addition, a summary of the trait means are presented in Supplemental Table 1.

536 **REFERENCES**

537 ALLEN, C. D., D. D. BRESHEARS, and N. G. MCDOWELL. 2015. ESA CENTENNIAL PAPER On
538 underestimation of global vulnerability to tree mortality and forest die-off from hotter
539 drought in the Anthropocene. Ecosphere 6: 1–55.
540 ANDEREGG, W. R. L. 2015. Spatial and temporal variation in plant hydraulic traits and their
541 relevance for climate change impacts on vegetation. New Phytol. 205: 1008–1014.
542 Available at: http://doi.wiley.com/10.1111/nph.12907.
543 ANDEREGG, W. R. L., T. KLEIN, M. K. BARTLETT, L. SACK, A. F. A. PELLEGRINI, and B. CHOAT.
544 2016. Meta-analysis reveals that hydraulic traits explain cross-species patterns of drought-
545 induced tree mortality across the globe. Proc. Natl. Acad. Sci. 113: 2–7.
546 BAILLIE, I. C., P. S. ASHTON, M. N. COURT, E. A. FITZPATRICK, J. TINSLEY, and J. A. R.
547 ANDERSON. 1987. Site characteristics and the distribution of tree species in mixed
548 dipterocarp forest on tertiary sediments in central sarawak, malaysia. J. Trop. Ecol. 3: 201–
549 220.
550 BARROS, F. DE V. ET AL. 2019. Hydraulic traits explain differential responses of Amazonian
551 forests to the 2015 El Niño-induced drought. New Phytol. 223: 1253–1266.
552 BARTLETT, M. K., T. KLEIN, S. JANSEN, B. CHOAT, and L. SACK. 2016. The correlations and
553 sequence of plant stomatal, hydraulic, and wilting responses to drought. Proc. Natl. Acad.
554 Sci. U. S. A. 113: 13098–13103.
555 BHASKAR, R., and D. D. ACKERLY. 2006. Ecological relevance of minimum seasonal water
556 potentials. Physiol. Plant. 127: 353–359. Available at: http://doi.wiley.com/10.1111/j.1399-
557 3054.2006.00718.x.
558 BLACKMAN, C. J., S. PFAUTSCH, B. CHOAT, S. DELZON, S. M. GLEASON, and R. A. DUURSMA.

2016. Toward an index of desiccation time to tree mortality under drought. Plant. Cell Environ. 39: 2342–2345. Available at: http://doi.wiley.com/10.1111/pce.12758.

BONGERS, F., L. POORTER, R. S. A. R. ROMPAEY, and M. P. E. PARREN. 1999. Distribution of twelve moist forest canopy tree species in Liberia and Côte d'Ivoire: response curves to a climatic gradient. J. Veg. Sci. 10: 371–382.

BRIENEN, R. J. W. ET AL. 2015. Long-term decline of the Amazon carbon sink. Nature 519: 344–348. Available at: http://dx.doi.org/10.1038/nature14283.

BRODRIBB, T. J., and H. COCHARD. 2009. Hydraulic Failure Defines the Recovery and Point of Death in Water-Stressed Conifers. Plant Physiol. 149: 575–584. Available at: http://www.plantphysiol.org/cgi/doi/10.1104/pp.108.129783.

CAVALERI, M. A., A. P. COBLE, M. G. RYAN, W. L. BAUERLE, H. W. LOESCHER, and S. F. OBERBAUER. 2017. Tropical rainforest carbon sink declines during El Niño as a result of reduced photosynthesis and increased respiration rates. New Phytol. 216: 136–149.

CHOAT, B. ET AL. 2012. Global convergence in the vulnerability of forests to drought. Nature 491: 752–755. Available at: http://dx.doi.org/10.1038/nature11688.

CONDIT, R. 1998. Tropical Forest Census Plots. Springer Verlag, Berlin, Heidelberg.

CONDIT, R., B. M. J. ENGELBRECHT, D. PINO, R. PEREZ, and B. L. TURNER. 2013. Species distributions in response to individual soil nutrients and seasonal drought across a community of tropical trees. Proc. Natl. Acad. Sci. 110: 5064–5068.

CONDIT, R., S. P. HUBBELL, and R. B. FOSTER. 1995. Mortality Rates of 205 Neotropical Tree and Shrub Species and the Impact of a Severe. Ecol. Monogr. 65: 419–439.

CONDIT, R., R. PEREZ, S. AGUILAR, and S. LAO. 2009. Sherman 6-ha Forest Census Plot Data. https://forestgeo.si.edu/sites/neotropics/sherman/sherman-plot-data.

582 CONDIT, R., R. PEREZ, S. AGUILAR, S. LAO, R. FOSTER, and S. HUBBELL. 2019a. Complete data
583 from the Barro Colorado 50-ha plot: 423617 trees, 35 years, v3, DataONE, Dataset,
584 https://doi.org/10.15146/5xcp-0d46.
585 CONDIT, R., R. PEREZ, S. AGUILAR, S. LAO, R. FOSTER, and S. P. HUBBELL. 2019b. BCI 50-ha
586 plot taxonomy.
587 CONDIT, R., R. PÉREZ, S. LAO, S. AGUILAR, and S. P. HUBBELL. 2017. Demographic trends and
588 climate over 35 years in the Barro Colorado 50 ha plot. For. Ecosyst. 4: 1–13.
589 CSARDI, G., and T. NEPUSZ. 2006. The igraph software package for complex network research.
590 InterJournal Complex Sys. 1695.
591 DICKMAN, L. T., N. G. MCDOWELL, C. GROSSIORD, A. D. COLLINS, B. T. WOLFE, M. DETTO, S. J.
592 WRIGHT, J. A. MEDINA-VEGA, D. GOODSMAN, A. ROGERS, S. P. SERBIN, J. WU, K. S. ELY,
593 S. T. MICHALETZ, C. XU, L. KUEPPERS, and J. Q. CHAMBERS. 2019. Homoeostatic
594 maintenance of nonstructural carbohydrates during the 2015–2016 El Niño drought across a
595 tropical forest precipitation gradient. Plant Cell Environ. 42: 1705–1714.
596 EAMUS, D., and L. PRIOR. 2001. Ecophysiology of trees of seasonally dry tropics: Comparisons
597 among phenologies.
598 ELY, K., A. ROGERS, S. SERBIN, J. WU, B. WOLFE, T. DICKMAN, A. COLLINS, M. DETTO, C.
599 GROSSIORD, N. MCDOWELL, and M. S. 2019. Leaf sample detail, Feb2016-May2016, PA-
600 SLZ, PA-PNM, PA-BCI: Panama. 1.0. NGEE Tropics Data Collection. (dataset).
601 ENGELBRECHT, B. M. J., L. S. COMITA, R. CONDIT, T. A. KURSAR, M. T. TYREE, B. L. TURNER,
602 and S. P. HUBBELL. 2007. Drought sensitivity shapes species distribution patterns in tropical
603 forests. Nature 447: 80–82.
604 GENTRY, A. H. 1988. Changes in Plant Community Diversity and Floristic Composition on

Environmental and Geographical Gradients. Ann. Missouri Bot. Gard. 75: 1–34.

GROSSIORD, C. ET AL. 2019. Precipitation mediates sap flux sensitivity to evaporative demand in the neotropics. Oecologia 191: 519–530.

HARTMANN, H., H. D. ADAMS, W. R. L. ANDEREGG, S. JANSEN, M. J. B. ZEPPEL, and I. I. W. ON T. MORTALITY. 2015. Research frontiers in drought- induced tree mortality : crossing scales and disciplines. New Phytol. 205: 965–969.

HUBBELL, S. P., R. B. FOSTER, S. T. O'BRIEN, K. E. HARMS, R. CONDIT, B. WECHSLER, S. J. WRIGHT, and S. LOO DE LAO. 1999. Light-gap disturbances, recruitment limitation, and tree diversity in a neotropical forest. Science (80-.). 283: 554–557.

KERSTIENS, G. 1996. Cuticular water permeability and its physiological significance. J. Exp. Bot. 47: 1813–1832. Available at: papers3://publication/uuid/F856AABA-4E74-4675-9452-31386BB17215.

KERSTIENS, G. 2006. Water transport in plant cuticles: An update. J. Exp. Bot. 57: 2493–2499.

KOIDE, R. T., R. H. ROBICHAUX, S. R. MORSE, and C. M. SMITH. 1991. Plant water status, hydraulic resistance and capacitance. *In* R. W. Pearcy, J. R. Ehleringer, H. Mooney, and P. W. Rundel (Eds.) Plant Physiological Ecology: Field Methods and Instrumentation. pp. 161–183, Chapman and Hall, New York, NY. Available at: papers3://publication/uuid/46B933D5-44CA-4F05-B1AC-D92686FF0D37.

MARTIN-STPAUL, N., S. DELZON, and H. COCHARD. 2017. Plant resistance to drought depends on timely stomatal closure. Ecol. Lett. 20: 1437–1447.

MCCULLOH, K. A., D. M. JOHNSON, F. C. MEINZER, and D. R. WOODRUFF. 2014. The dynamic pipeline: hydraulic capacitance and xylem hydraulic safety in four tall conifer species. Plant. Cell Environ. 37: 1171–1183. Available at:

http://eutils.ncbi.nlm.nih.gov/entrez/eutils/elink.fcgi?dbfrom=pubmed&id=24289816&retmode=ref&cmd=prlinks.

McDowell, N. et al. 2018. Drivers and mechanisms of tree mortality in moist tropical forests. New Phytol. 219: 851–869.

Meinzer, F. C., S. A. James, G. Goldstein, and D. R. Woodruff. 2003. Whole-tree water transport scales with sapwood capacitance in tropical forest canopy trees. Plant. Cell Environ. 26: 1147–1155. Available at: http://onlinelibrary.wiley.com/doi/10.1046/j.1365-3040.2003.01039.x/full.

Meinzer, F. C., D. M. Johnson, B. Lachenbruch, K. A. McCulloh, and D. R. Woodruff. 2009. Xylem hydraulic safety margins in woody plants: coordination of stomatal control of xylem tension with hydraulic capacitance. Funct. Ecol. 23: 922–930. Available at: http://doi.wiley.com/10.1111/j.1365-2435.2009.01577.x.

Meinzer, F. C., and K. A. McCulloh. 2013. Xylem recovery from drought-induced embolism: where is the hydraulic point of no return? Tree Physiol. 33: 331–334. Available at: http://eutils.ncbi.nlm.nih.gov/entrez/eutils/elink.fcgi?dbfrom=pubmed&id=23612243&retmode=ref&cmd=prlinks.

Nardini, A., M. Battistuzzo, and T. Savi. 2013. Shoot desiccation and hydraulic failure in temperate woody angiosperms during an extreme summer drought. New Phytol. 200: 322–329.

Nardini, A., E. Gortan, M. Ramani, and S. Salleo. 2008. Heterogeneity of gas exchange rates over the leaf surface in tobacco: An effect of hydraulic architecture? Plant, Cell Environ. 31: 804–812.

Osazuwa-Peters, O., A. E. Zanne, and P. contributors. 2011. Wood density.

651 PrometheusWiki. Available at: http://prometheuswiki.publish.csiro.au/tiki-
652 index.php?page=Wood+density+protocol.
653 PEREIRA, L., R. S. OLIVEIRA, P. R. L. BITTENCOURT, M. B. M. JUNIOR, and F. V. BARROS. 2016.
654 Plant pneumatics : stem air flow is related to embolism – new perspectives on methods in
655 plant hydraulics Methods Plant pneumatics : stem air flow is related to embolism – new
656 perspectives on methods in plant hydraulics. New Phytol. 357–370.
657 PIVOVAROFF, A. L., V. M. W. COOK, and L. S. SANTIAGO. 2018. Stomatal behavior and stem
658 xylem traits are coordinated for woody plant species under exceptional drought conditions.
659 Plant. Cell Environ. 41: 2617–2626. Available at: http://doi.wiley.com/10.1111/pce.13367.
660 PIVOVAROFF, A. L., S. C. PASQUINI, M. E. DE GUZMAN, K. P. ALSTAD, J. S. STEMKE, and L. S.
661 SANTIAGO. 2016. Multiple strategies for drought survival among woody plant species.
662 Funct. Ecol. 30: 517–526. Available at: http://doi.wiley.com/10.1111/1365-2435.12518.
663 POWERS, J. S. ET AL. 2020. A catastrophic tropical drought kills hydraulically vulnerable tree
664 species. Glob. Chang. Biol. 26: 3122–3133.
665 PRATT, R. B., and A. L. JACOBSEN. 2017. Conflicting demands on angiosperm xylem: Tradeoffs
666 among storage, transport and biomechanics. Plant Cell Environ. 40: 897–913.
667 PRATT, R. B., A. L. JACOBSEN, F. W. EWERS, and S. D. DAVIS. 2007. Relationships among xylem
668 transport, biomechanics and storage in stems and roots of nine Rhamnaceae species of the
669 California chaparral. New Phytol. 174: 787–798. Available at:
670 http://doi.wiley.com/10.1111/j.1469-8137.2007.02061.x.
671 R CORE TEAM. 2020. R: A language and environment for statistical computing. Available at:
672 https://www.r-project.org/.
673 ROSAS, T., M. MENCUCCINI, J. BARBA, H. COCHARD, S. SAURA-MAS, and J. MARTÍNEZ-VILALTA.

2019. Adjustments and coordination of hydraulic, leaf and stem traits along a water availability gradient. New Phytol. 223: 632–646.

SANTIAGO, L. S., M. E. DE GUZMAN, C. BARALOTO, J. E. VOGENBERG, M. BRODIE, B. HÉRAULT, C. FORTUNEL, and D. BONAL. 2018. Coordination and trade-offs among hydraulic safety, efficiency and drought avoidance traits in Amazonian rainforest canopy tree species. New Phytol. 218: 1015–1024.

SAVI, T., V. L. LOVE, A. DAL BORGO, S. MARTELLOS, and A. NARDINI. 2017. Morpho-anatomical and physiological traits in saplings of drought-tolerant Mediterranean woody species. Trees - Struct. Funct. 31: 1137–1148.

SCHOLZ, F. G., S. J. BUCCI, G. GOLDSTEIN, F. C. MEINZER, A. C. FRANCO, and F. MIRALLES-WILHELM. 2007. Biophysical properties and functional significance of stem water storage tissues in Neotropical savanna trees. Plant, Cell Environ. 30: 236–248.

SERGENT, A. S., S. A. VARELA, T. S. BARIGAH, E. BADEL, H. COCHARD, G. DALLA-SALDA, S. DELZON, M. E. FERNÁNDEZ, J. GUILLEMOT, J. GYENGE, L. J. LAMARQUE, A. MARTINEZ-MEIER, P. ROZENBERG, J. M. TORRES-RUIZ, and N. K. MARTIN-STPAUL. 2020. A comparison of five methods to assess embolism resistance in trees. For. Ecol. Manage. 468: 118175. Available at: https://doi.org/10.1016/j.foreco.2020.118175.

SHINOZAKI, K., K. YODA, K. HOZUMI, and T. KIRA. 1964. A quantitative analysis of plant form - The pipe model theory. Japanese J. Ecol. 14: 133–139. Available at: papers3://publication/uuid/FAFC0D17-280E-4183-8844-906E21900329.

SPERRY, J. S., and D. M. LOVE. 2015. What plant hydraulics can tell us about responses to climate-change droughts.

TAN, F., H. SONG, P. FU, Y. CHEN, Z. SIDDIQ, and K. CAO. 2020. Agricultural and Forest

Meteorology Hydraulic safety margins of co-occurring woody plants in a tropical karst forest experiencing frequent extreme droughts. Agric. For. Meteorol. 292–293: 108107. Available at: https://doi.org/10.1016/j.agrformet.2020.108107.

TRENBERTH, K. E., A. DAI, G. VAN DER SCHRIER, P. D. JONES, J. BARICHIVICH, K. R. BRIFFA, and J. SHEFFIELD. 2014. Global warming and changes in drought. Nat. Clim. Chang. 4: 17–22.

TRIFILÒ, P., A. NARDINI, M. A. L. GULLO, P. M. BARBERA, T. SAVI, and F. RAIMONDO. 2015. Diurnal changes in embolism rate in nine dry forest trees: Relationships with species-specific xylem vulnerability, hydraulic strategy and wood traits. Tree Physiol. 35: 694–705.

TRUGMAN, A. T., L. D. L. ANDEREGG, J. S. SPERRY, Y. WANG, M. VENTURAS, and W. R. L. ANDEREGG. 2019. Leveraging plant hydraulics to yield predictive and dynamic plant leaf allocation in vegetation models with climate change. Glob. Chang. Biol. 25: 4008–4021.

TRUGMAN, A. T., L. D. L. ANDEREGG, B. T. WOLFE, B. BIRAMI, N. K. RUEHR, M. DETTO, M. K. BARTLETT, and W. R. L. ANDEREGG. 2019. Climate and plant trait strategies determine tree carbon allocation to leaves and mediate future forest productivity. Glob. Chang. Biol. 25: 3395–3405.

TYREE, M. T., and F. W. EWERS. 1991. The Hydraulic Architecture of Trees and Other Woody Plants. New Phytol. 119: 345–360. Available at: papers3://publication/uuid/DC2544F2-0DE1-4996-9B9A-E5F65AD3F932.

WILLIAMSON, G. B., and M. C. WIEMANN. 2010. Measuring wood specific gravity…Correctly. Am. J. Bot. 97: 519–524. Available at: http://eutils.ncbi.nlm.nih.gov/entrez/eutils/elink.fcgi?dbfrom=pubmed&id=21622413&retmode=ref&cmd=prlinks.

720 WOLFE, B. T. 2017. Retention of stored water enables tropical tree saplings to survive extreme
721 drought conditions. Tree Physiol. 37: 469–480.
722 WOLFE, B., J. WU, K. ELY, S. ERBIN, A. ROGERS, T. DICKMAN, A. COLLINS, M. DETTO, C.
723 GROSSIORD, N. MCDOWELL, and S. MICHALETZ. 2019. Leaf water potential, Feb2016-
724 May2016, PA-SLZ, PA-PNM, PA-BCI: Panama. 1.0. NGEE Tropics Data Collection.
725 (dataset).
726

727 **Table 1.** 27 canopy tree species from Parque Natural Metropolitano (*n* = 9), Barro Colorado
728 Island (*n*=9), and Fort San Lorenzo (*n* = 9) used for this study, with mean sapwood density and
729 standard deviation, and leaf phenology.

Site	Species	Sapwood density ± SD ($g\ cm^{-3}$)	Deciduous/Evergreen
Parque Natural Metropolitano	*Albizia adinocephala*	0.62 ± 0.08	Deciduous
	Anacardium excelsum	0.41 ± 0.054	Brevideciduous
	Pittoniotis trichantha	0.46 ± 0.041	Facultative deciduous
	Calycophyllum candidissimum	0.60 ± 0.04	Evergreen
	Castilla elastica	0.42 ± 0.034	Facultative deciduous
	Cordia alliodora	0.36 ± 0.02	Facultative deciduous
	Ficus insipida	0.45 ± 0.061	Brevideciduous
	Luehea seemannii	0.33 ± 0.045	Facultative deciduous
	Pseudobombax septenatum	0.39 ± 0.074	Obligate deciduous
Barro Colorado Island	*Alseis blackiana*	0.47 ± 0.013	Facultative deciduous
	Gustavia superba	0.47 ± 0.041	Evergreen
	Hura crepitans	0.45 ± 0.028	Facultative deciduous
	Inga pezizifera	0.59 ± 0.019	Evergreen
	Miconia argentea	0.56 ± 0.037	Evergreen
	Schizolobium parahyba	0.42 ± 0.102	Deciduous
	Simarouba amara	0.46 ± 0.01	Evergreen
	Spondias radlkoferi	0.41 ± 0.022	Facultative deciduous
	Tabebuia rosea	o.46 ± 0.014	Facultative deciduous
Fort San Lorenzo	*Apeiba membranaceae*	0.35 ± 0.034	Facultative deciduous
	Carapa guianensis	0.46 ± 0.028	Facultative deciduous
	Guatteria dumetorum	0.48 ± 0.059	Evergreen
	Miconia minutiflora	0.56 ± 0.022	Evergreen
	Tachigali versicolor	0.71 ± 0.019	Evergreen
	Terminalia amazonia	0.68 ± 0.027	Brevideciduous
	Tocoyena pittieri	0.69 ± 0.016	Evergreen
	Virola multiflora	0.50 ± 0.026	Evergreen
	Vochysia ferruginea	0.53 ± 0.017	Evergreen

730

731 **Table 2.** Measured traits with their corresponding symbol and units, along with the descriptors of
732 the trait network across 27 study species from 3 sites in Panama with varying mean annual
733 precipitation. The degree of network centrality (D) is defined as the number of edges per node.
734 The weighted degree of network centrality (D_W) is defined as the sum of absolute values for all
735 significant coefficients of correlation for a node.

Trait	Symbol	Units	D	D_W
Path 1				
Turgor loss point	π_{TLP}	MPa	2	0.98
Instantaneous mortality rate			2	1.14
Elbow of cumulative water release curve	C_{ELBOW}	MPa	2	1.26
Sapwood density	ρ_{SW}	g cm^{-3}	2	1.02
Minimum seasonal water potential	Ψ_{MIN}	MPa	4	2.7
Minimum seasonal water potential minus maximum seasonal water potential	$\Delta\Psi$	MPa	4	2.75
Sapwood capacitance	C_{SW}	kg m^{-3} MPa^{-1}	5	2.56
Minimum seasonal water potential minus elbow of cumulative water release curve	$\Psi_{MIN} - C_{ELBOW}$	MPa	5	2.81
Minimum seasonal water potential minus turgor loss point	$\Psi_{MIN} - \pi_{TLP}$	MPa	6	3.58
Path 2				
Leaf dry matter content	LDMC	g g^{-1}	1	0.68
Optimal moisture			1	0.48
Leaf mass per area	LMA	g m^{-2}	2	1.12
Leaf area to sapwood area ratio	A_L:A_{SW}	m^2 m^{-2}	2	0.92

736

737 **Figure captions**

738 **Figure 1**. Map of North and South America with the location of Panama outlined in black (white
739 inset box), with a close-up of the Republic of Panama and the three study sites, Parque Natural
740 Metropolitano (PNM; light blue), Barro Colorado Island (BCI; medium blue), and Fort San
741 Lorenzo (SLZ; dark blue) (panel b). These sites capture a precipitation gradient across the
742 Isthmus of Panama, as presented by the differences in total monthly precipitation (mm) as well
743 as long-term differences in total annual precipitation (mm/year) from 1997-2019. Seasonal
744 patterns reveal the majority of rainfall occurs during the wet season (May – November), and
745 long-term patterns demonstrate that of the three study sites, SLZ has the highest precipitation and
746 PNM has the lowest precipitation.
747
748 **Figure 2**. Minimum seasonal water potential (Ψ_{MIN}; MPa), the difference between the minimum
749 seasonal water potential and maximum seasonal water potential ($\Delta\Psi$; MPa), turgor loss point
750 (π_{TLP}; MPa), the difference between the minimum seasonal water potential and turgor loss point
751 ($\Psi_{MIN} - \pi_{TLP}$; MPa), the "elbow" of the cumulative water release curve (C_{ELBOW}; MPa), and the
752 difference between the minimum seasonal water potential and the "elbow" of the cumulative
753 water release curve ($\Psi_{MIN} - C_{ELBOW}$; MPa) measured at Parque Natural Metropolitano (PNM;
754 light blue), Barro Colorado Island (BCI; medium blue), and Fort San Lorenzo (SLZ; dark blue)
755 in Panama during the 2015 – 2016 El Niño. The boxplots display the median as a bold horizontal
756 line, with colored hinges above and below the median to illustrate the 25th and 75th percentile.
757 Outliers, values more than 1.5 times the inter-quartile range, are displayed as individual black
758 points. The raw data points are overlaid on the boxplots as color-filled points. There were no
759 significant differences between sites ($\alpha = 0.05$) for any trait.
760
761 **Figure 3.** Leaf area to sapwood area ratio (A_L:A_{SW}; $m^2\ m^{-2}$), leaf mass per area (LMA; $g\ m^{-2}$),
762 leaf dry matter content (LDMC; $g\ g^{-1}$), sapwood density (ρ_{SW}; g cm-3), and sapwood capacitance
763 (C_{SW}; $kg\ m^{-3}\ MPa^{-1}$) measured at Parque Natural Metropolitano (PNM; light blue), Barro
764 Colorado Island (BCI; medium blue), and Fort San Lorenzo (SLZ; dark blue) in Panama during
765 the 2015 – 2016 El Niño. The boxplots display the median as a bold horizontal line, with colored
766 hinges above and below the median to illustrate the 25th and 75th percentile. Outliers, values
767 more than 1.5 times the inter-quartile range, are displayed as individual black points. The raw

768 data points are overlaid on the boxplots as color-filled points. There were no significant
769 differences between sites ($\alpha = 0.05$) for any trait.
770
771 **Figure 4.** Optimal moisture and instantaneous mortality rate for species measured at Parque
772 Natural Metropolitano (PNM; light blue), Barro Colorado Island (BCI; medium blue), and Fort
773 San Lorenzo (SLZ; dark blue) in Panama during the 2015 – 2016 El Niño. Mortality rates were
774 calculated from the 2010 and 2015 BCI censuses, and filtered to include trees with a minimum
775 diameter at breast height (DBH) of 20 cm. The boxplots display the median as a bold horizontal
776 line, with colored hinges above and below the median to illustrate the 25th and 75th percentile.
777 Outliers, values more than 1.5 times the inter-quartile range, are displayed as individual black
778 points. The raw data points are overlaid on the boxplots as color-filled points. There were no
779 significant differences between sites ($\alpha = 0.05$) for any trait.
780
781 **Figure 5.** Trait network analysis for species measured at Parque Natural Metropolitano, Barro
782 Colorado Island, and Fort San Lorenzo in Panama during the 2015 – 2016 El Niño. Each trait
783 represents a node in the network, and each significant correlation represents an edge in the
784 network. Corresponding trait names for each node, along with the degree and weighted degree of
785 network centrality, are in Table 2.
786
787 **Figure 6**. Correlation between species-specific optimal moisture and leaf area to sapwood area
788 ratio (A_L:A_{SW}; m m^{-2}) measured at Parque Natural Metropolitano (PNM; light blue), Barro
789 Colorado Island (BCI; medium blue) and Fort San Lorenzo (SLZ; dark blue) in Panama during
790 the 2015 – 2016 El Niño. Leaf habit (i.e. deciduousness) is indicated by the symbol shape.
791 Higher optimal moisture values mean a species is more highly associated with wet sites and
792 therefore more moisture dependent.
793

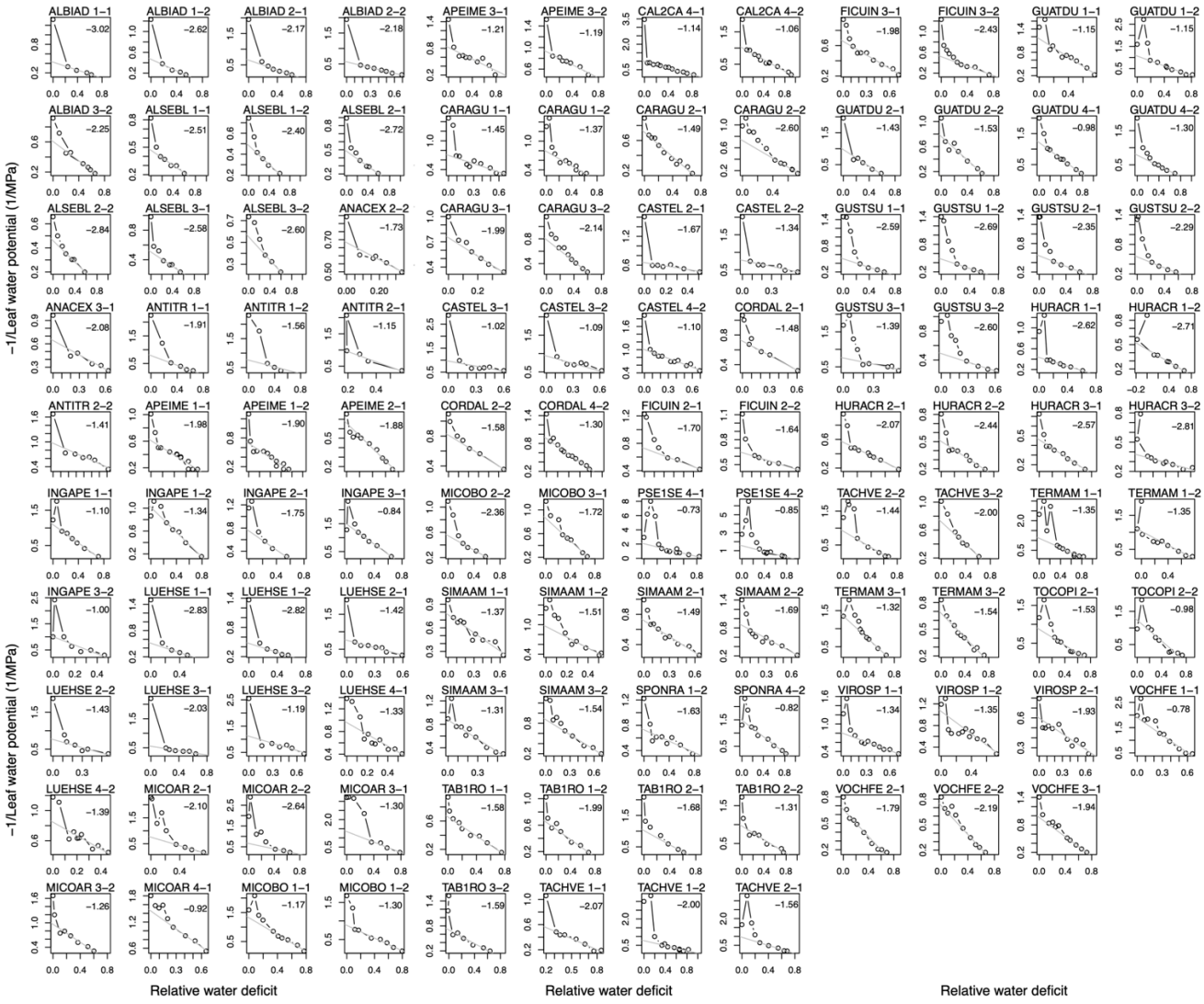

Supplemental Figure 1. Raw pressure volume curves measured for 27 canopy tree species at San Lorenzo, Barro Colorado Island, and Parque Natural Metropolitano in Panama.

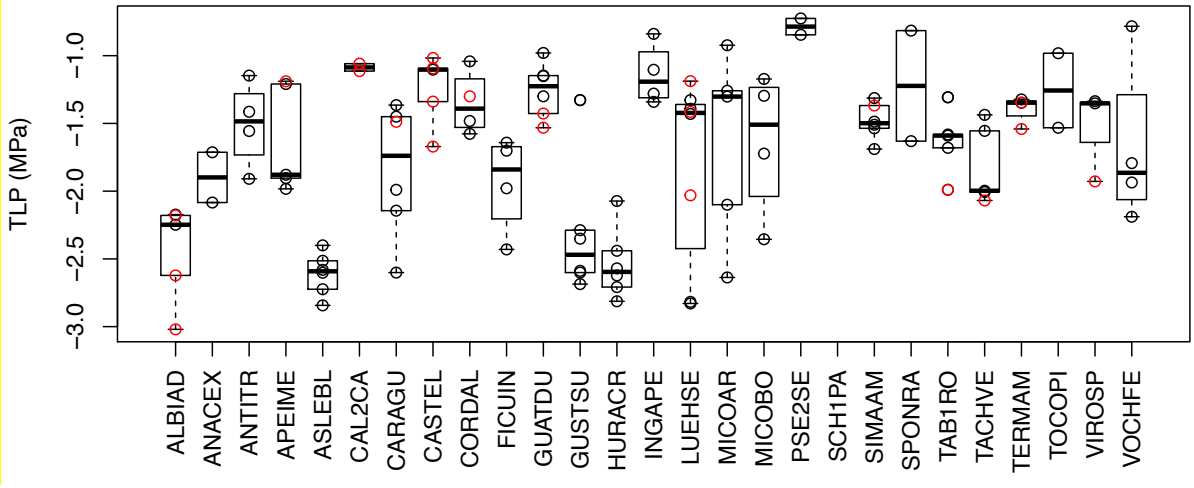

Supplemental Figure 2. Box plots of turgor loss points (TLP) derived from pressure-volume curves for each study species. The boxplots display the median as a bold horizontal line, with hinges above and below the median to illustrate the 25th and 75th percentile. Each overlayed circle represents a TLP value, with red circles representing the values from pressure-volume curves with just one point above the TLP. There is no trend for artificially low TLP in the curves with just one point as the red circles are above the median as often as below.

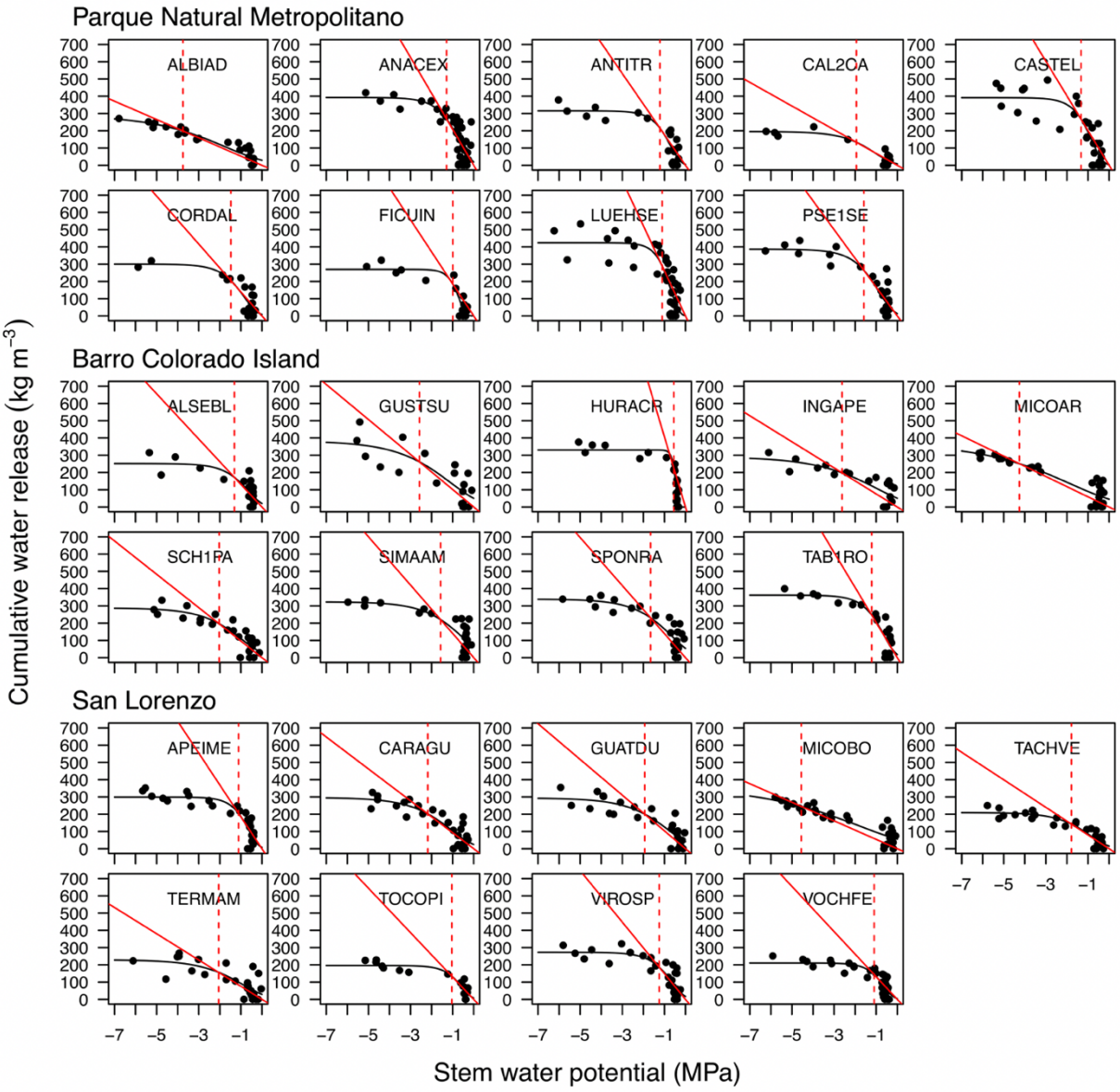

Supplemental Figure 3. Cumulative water release curves measured for 27 canopy tree species at San Lorenzo, Barro Colorado Island, and Parque Natural Metropolitano in Panama.

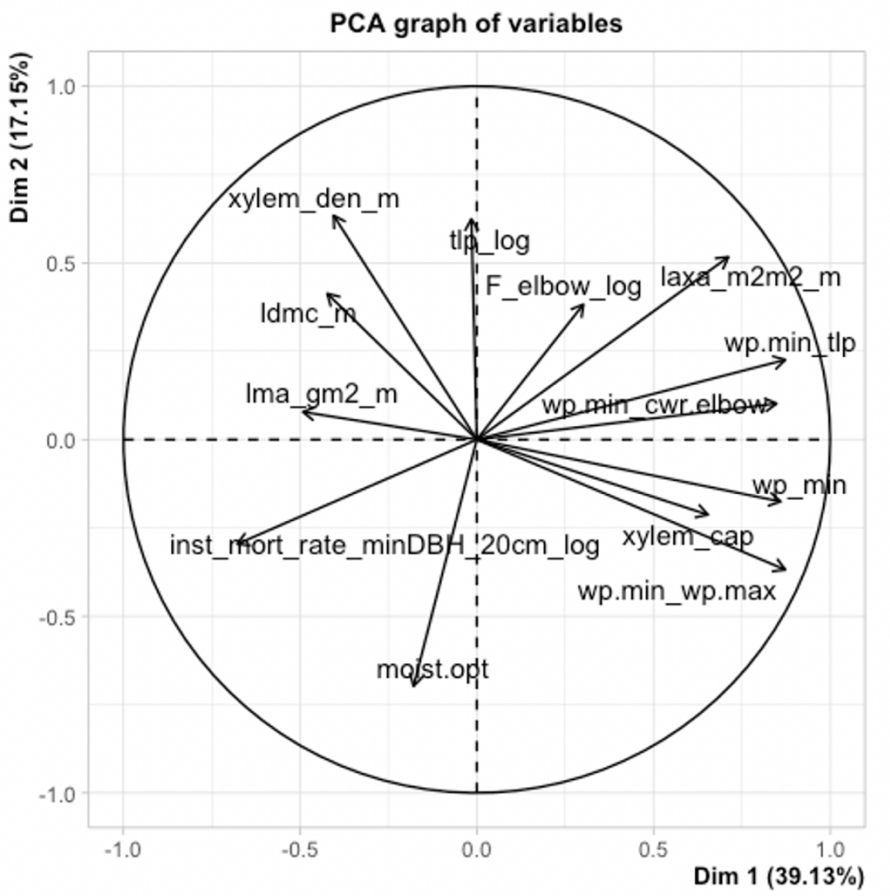

Supplemental Figure 4. We conducted a principal components analysis in R with the "stats" package and the "princomp" function. We included 11 of the 13 variables from our network analysis, with the 2 excluded variables being optimal moisture and mortality rate. With this analysis, we found that two dimensions explained 56.2% of the variance.

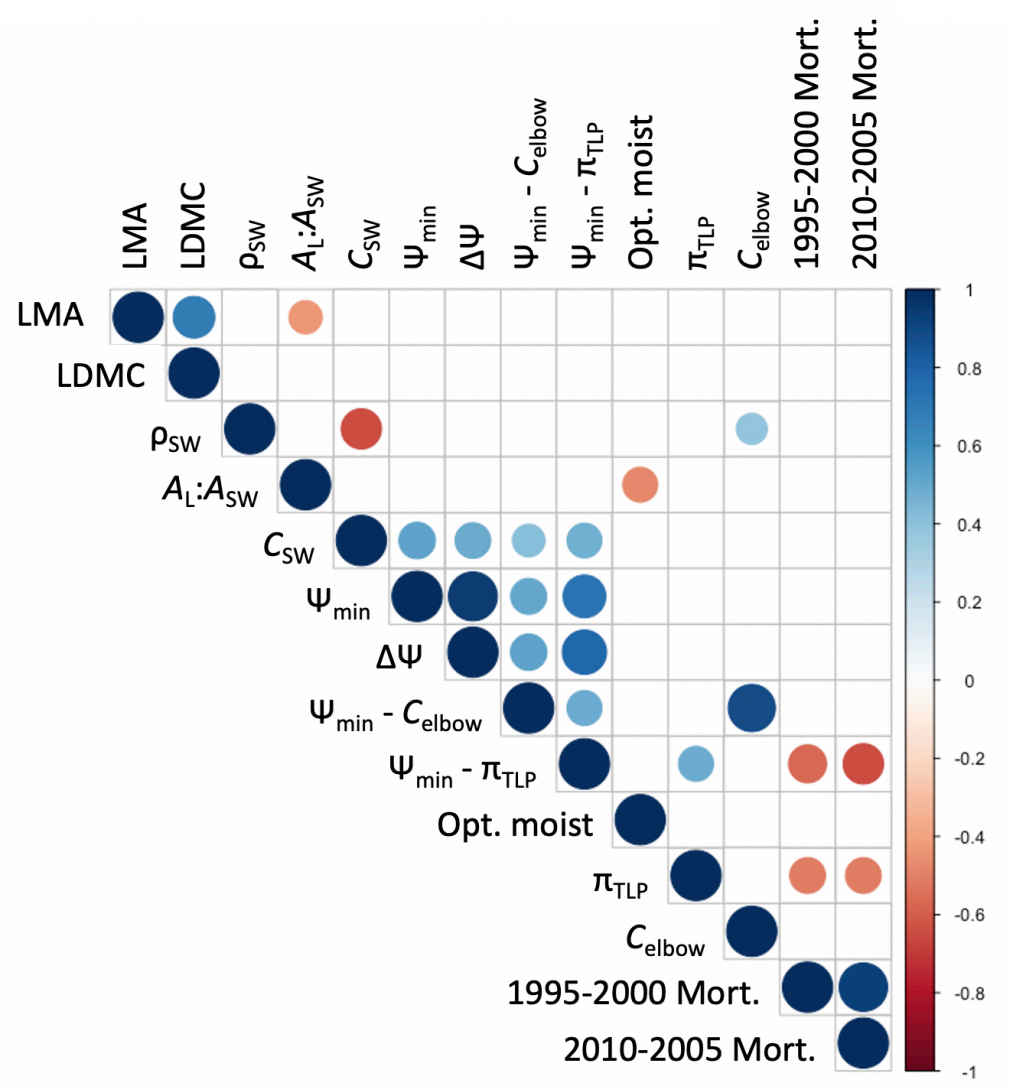

Supplemental Figure 5. Correlogram of traits for species measured at Parque Natural Metropolitano (PNM; light blue), Barro Colorado Island (BCI; medium blue), and Fort San Lorenzo (SLZ; dark blue) in Panama during the 2015 – 2016 El Niño. Mortality rates were calculated from the 2010 and 2015 BCI censuses, as well as the 1995 and 2000 BCI censuses, and filtered to include trees with a minimum diameter at breast height (DBH) of 20 cm. There was an El Niño event in 1997-1998, so this second mortality rate captures mortality trends in response to moisture stress. Only traits with a significant correlation ($p < 0.05$) have a colored circle. Blue indicates a positive correlation, while red indicates a negative correlation; the color intensity corresponds to the r value as shown by the gradient on the right. Abbreviations and units are found in Table 2.

Supplemental Table 1. Summary of mean ± standard deviation for leaf mass per area (LMA), leaf dry matter content (LDMC), turgor loss point (π_{TLP}), leaf area to sapwood area ratio (A_L:A_{SW}), the "elbow" of the cumulative water release curve (C_{elbow}), sapwood capacitance (C_{SW}), minimum seasonal water potential (Ψ_{MIN}), the difference between the minimum and maximum seasonal water potential ($\Delta\Psi$), Ψ_{MIN} minus C_{elbow} ($\Psi_{MIN} - C_{elbow}$), Ψ_{MIN} minus π_{TLP} ($\Psi_{MIN} - \pi_{TLP}$), and the moisture optimum for each species.

Species	LMA g m^{-2}	LDMC g g^{-1}	π_{TLP} MPa	A_L:A_{SW} m^2 m^{-2}	C_{elbow} MPa	C_{SW} kg m^{-3} MPa^{-1}	Ψ_{MIN} MPa	$\Delta\Psi$ MPa	Ψ_{MIN}-C_{elbow} MPa	Ψ_{MIN} - π_{TLP} MPa	Moisture optimum
Albizia adinocephala	48.46 ± 11.62	0.3389 ± 0.0717	-2.448 ± 0.369	4009.14 ± 3006.21	-3.75	198.92	-2.8	-1.9	0.949	-0.352	-2.23
Alseis blackiana	24.55 ± 3.78	0.2684 ± 0.0375	-2.611 ± 0.156	NA ± NA	-1.31	171.93	-2.8	-2	-1.49	-0.189	-2.04
Anacardium excelsum	89.77 ± 15.91	0.4244 ± 0.0425	-1.994 ± 0.248	7003.14 ± 1935.85	-1.29	267.93	-2	-1.55	-0.714	-0.006	-1.77
Pittoniotis trichantha	49.04 ± 12.28	0.2961 ± 0.0239	-1.33 ± 0.481	7514.58 ± 559.81	-1.21	215.02	-2.5	-2.05	-1.287	-1.17	-2.72
Apeiba membranacea	68.57 ± 17.71	0.337 ± 0.0615	-1.633 ± 0.398	3516.62 ± 852.12	-1.11	204.05	-2	-1.6	-0.895	-0.367	1.01
Calycophyllum candidissimum	61.07 ± 20.73	0.298 ± 0.0735	-1.163 ± 0.136	10882.37 ± 4702.27	-1.94	133.47	-3.7	-3.4	-1.756	-2.537	-2.12
Carapa guianensis	134.47 ± 8.51	0.4508 ± 0.0328	-1.328 ± 0.155	1711.06 ± 334.3	-2.18	202.08	-2.05	-1.6	0.135	-0.722	1.73
Castilla elastica	68.73 ± 12.45	0.2996 ± 0.0316	-1.245 ± 0.267	6649.2 ± 2758.25	-1.33	267.16	-2.3	-1.9	-0.971	-1.055	-1.74
Cordia alliodora	38 ± 7.27	0.2478 ± 0.0334	-1.238 ± 0.195	4130.55 ± 2104	-1.48	204.95	-2.95	-1.95	-1.474	-1.712	0.05
Ficus insipida	104.45 ± 30.15	0.3215 ± 0.0753	-1.938 ± 0.359	2822.59 ± 531.14	-0.99	184.21	-2.85	-2.35	-1.858	-0.912	-0.01
Guatteria dumetorum	64.89 ± 4.59	0.364 ± 0.0302	-1.256 ± 0.203	3382.07 ± 542.45	-1.94	200.25	-2.55	-2.15	-0.614	-1.294	0.52
Gustavia superba	35.94 ± 5.3	0.2393 ± 0.0456	-2.248 ± 0.54	9313.9 ± 4566.58	-2.58	261.44	-1.95	-1.15	0.627	0.298	0.08
Hura crepitans	54.48 ± 5.77	0.2869 ± 0.0091	-2.538 ± 0.26	3076.15 ± 823.34	-0.55	225.27	--	--	--	--	0.6
Inga pezizifera	41.15 ± 6.72	0.3522 ± 0.0307	-1.262 ± 0.333	6210.98 ± 1256.12	-2.62	198.22	-2.1	-1.45	0.524	-0.838	1.04
Luehea seemannii	70.87 ± 20.8	0.3733 ± 0.0556	-1.804 ± 0.676	6814.62 ± 2374.81	-1.11	289.27	-2.9	-2.5	-1.793	-1.096	-0.33
Miconia argentea	58.5 ± 8.12	0.2997 ± 0.0475	-1.802 ± 0.738	9585.03 ± 358.38	-4.26	251.28	-2.3	-1.95	1.961	-0.498	-0.42
Miconia minutiflora	73.72 ± 5.76	0.4079 ± 0.0168	-1.542 ± 0.574	3605.61 ± 261.21	-4.55	245.07	-2.7	-2.25	1.853	-1.158	-0.6
Pseudobombax septenatum	81.88 ± 19.34	0.3616 ± 0.071	-0.786 ± 0.086	5381.67 ± 3810.09	-1.58	263.79	-1.3	-0.8	0.283	-0.514	-0.44
Schizolobium parahyba	71.97 ± 8.73	0.3401 ± 0.0404	-1.218 ± 0.006	3560.68 ± 1988.37	-2.03	196.35	--	--	--	--	0.35
Simarouba amara	108.54 ± 18.25	0.3785 ± 0.0549	-1.484 ± 0.133	3781.5 ± 209.21	-1.57	220.53	-2.8	-2.3	-1.227	-1.316	1.39
Spondias radlkoferi	56.06 ± 18.22	0.2874 ± 0.06	-1.223 ± 0.577	4342.14 ± 313.5	-1.66	231.19	--	--	--	--	0.86
Tabebuia rosea	58.9 ± 3.45	0.3731 ± 0.0308	-1.449 ± 0.368	3149.39 ± 823.83	-1.22	247.26	--	--	--	--	-0.31
Tachigali versicolor	76.95 ± 5.33	0.454 ± 0.0633	-1.813 ± 0.294	5623.98 ± 1061.57	-1.79	142.69	-2.9	-2.5	-1.114	-1.087	-0.63
Terminalia amazonia	78.92 ± 5.92	0.388 ± 0.0056	-1.569 ± 0.411	4963.26 ± 885.54	-2.06	156.34	-2.9	-2.4	-0.845	-1.331	-3
Tocoyena pittieri	54.55 ± 7.28	0.3152 ± 0.0204	-1.257 ± 0.389	5736.19 ± 2927.79	-1.04	133.75	-2.45	-2.05	-1.412	-1.193	0.67
Virola multiflora	111.72 ± 8.88	0.3849 ± 0.02	-1.792 ± 0.576	2939.04 ± 309.58	-1.25	186.22	-3.5	-3.1	-2.252	-1.708	0.72
Vochysia ferruginea	96.02 ± 10.3	0.3351 ± 0.0382	-1.466 ± 0.71	5441.27 ± 4689.5	-1.1	143.71	-2.75	-2.25	-1.652	-1.284	-0.32

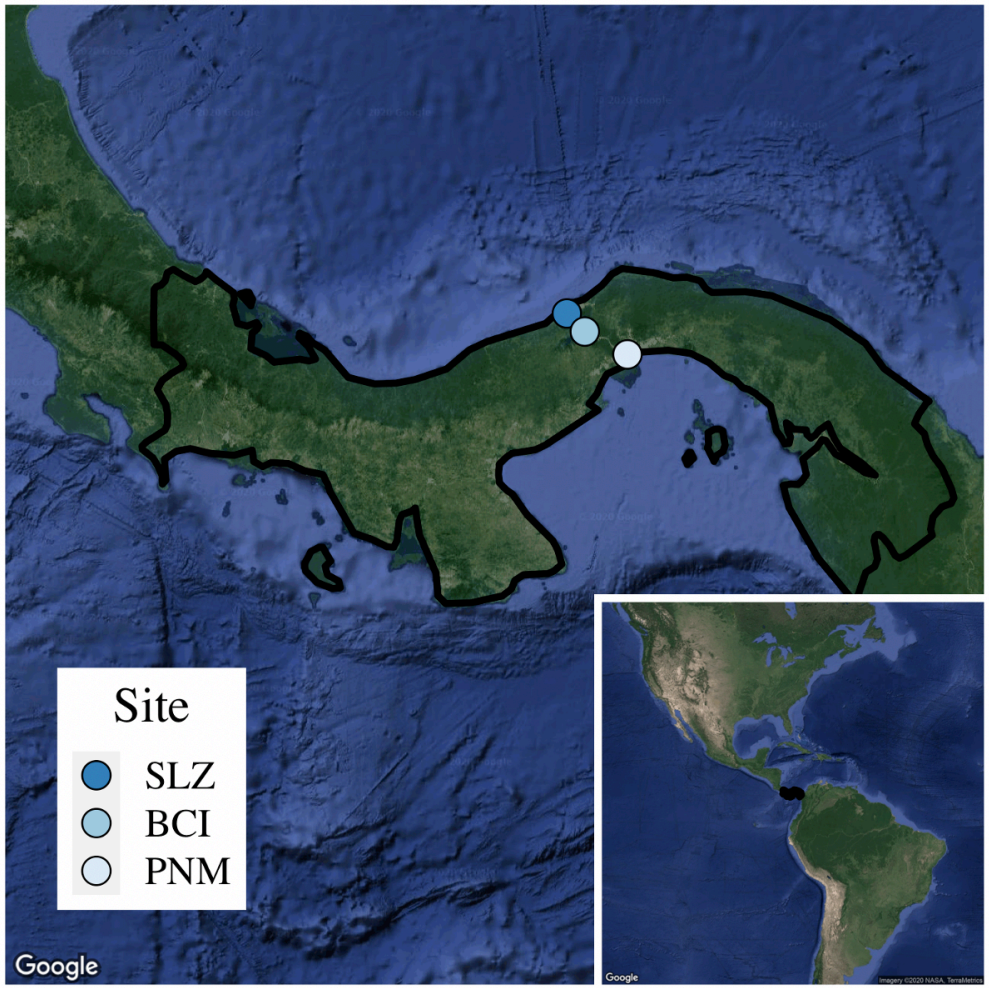
Site
SLZ
BCI
PNM
Google
Google

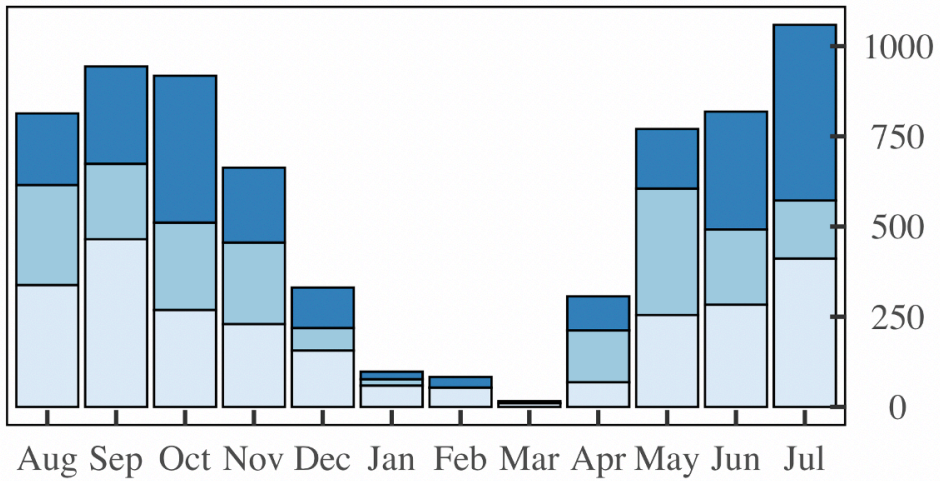
1000
750
500
250
0
Aug Sep Oct Nov Dec Jan Feb Mar Apr May Jun Jul
Month
Total monthly precipitation (mm)

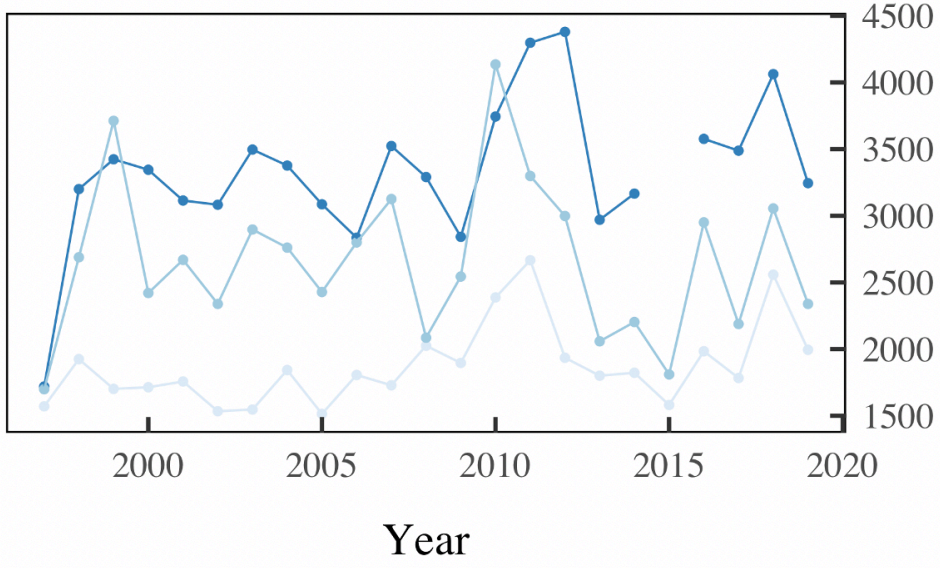
4500
4000
3500
3000
2500
2000
1500
2000 2005 2010 2015 2020
Year
Total annual precipitation (mm/year)

Ψ_{MIN} (MPa)
π_{TLP} (MPa)
C_{ELBOW} (MPa)
$\Delta\Psi$ (MPa)
$\Psi_{MIN} - \pi_{TLP}$ (MPa)
$\Psi_{MIN} - C_{ELBOW}$ (MPa)
-2.0
-3.0
-1.0
-2.0
-2.5
-1.0
-1.5
-2.0
-4.0
-1.0
-1.5
-2.0
-2.5
-3.0
-3.5
0.0
-0.5
-1.0
-1.5
-2.0
-2.5
2.0
1.0
0.0
-1.0
-2.0
PNM
BCI
SLZ
PNM
BCI
SLZ
Site
Site

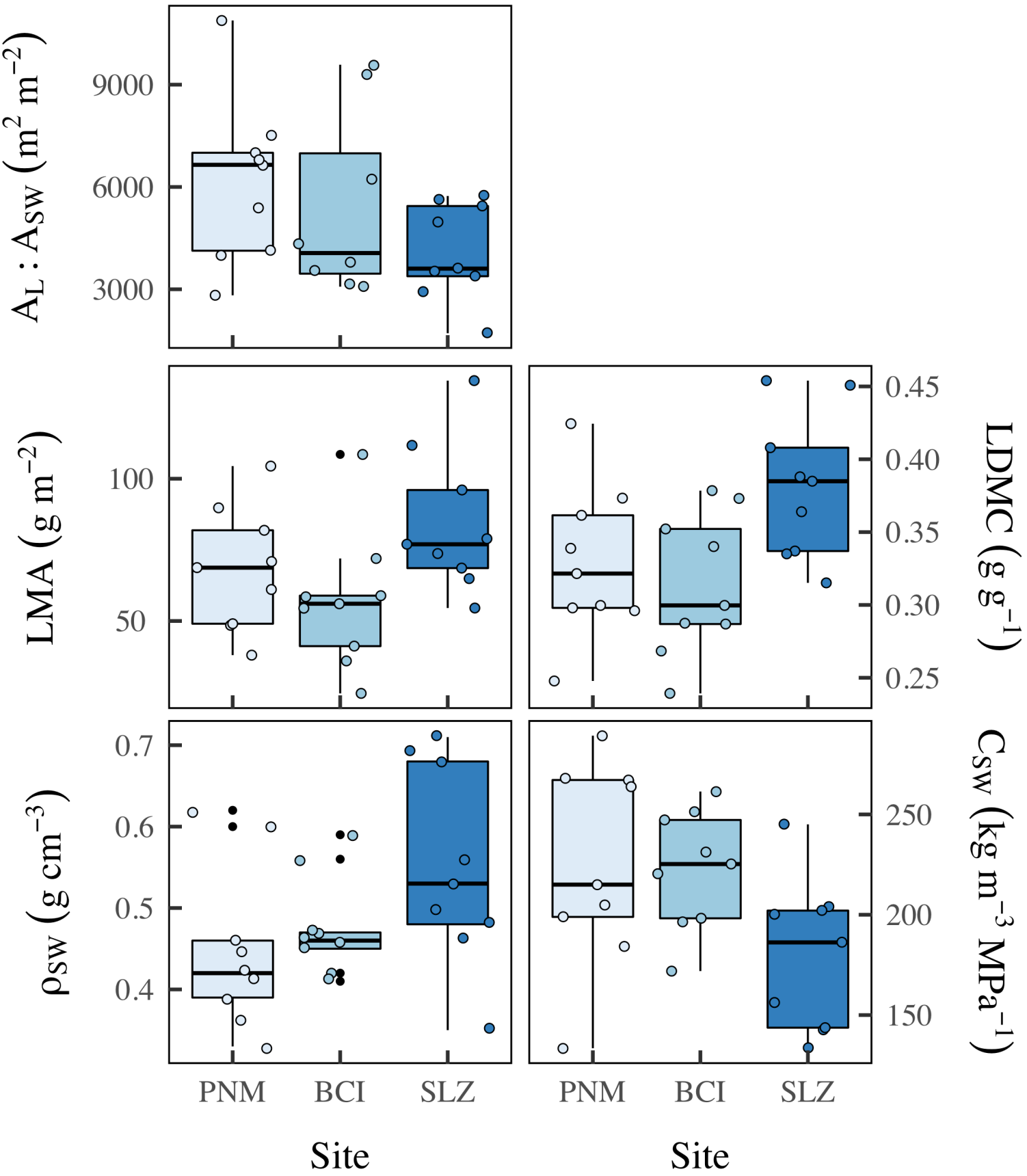
$A_L : A_{SW}$ (m^2 m^{-2})
9000
6000
3000
LMA (g m^{-2})
100
50
LDMC (g g^{-1})
0.45
0.40
0.35
0.30
0.25
ρ_{SW} (g cm^{-3})
0.7
0.6
0.5
0.4
C_{SW} (kg m^{-3} MPa^{-1})
250
200
150
PNM
BCI
SLZ
Site
PNM
BCI
SLZ
Site

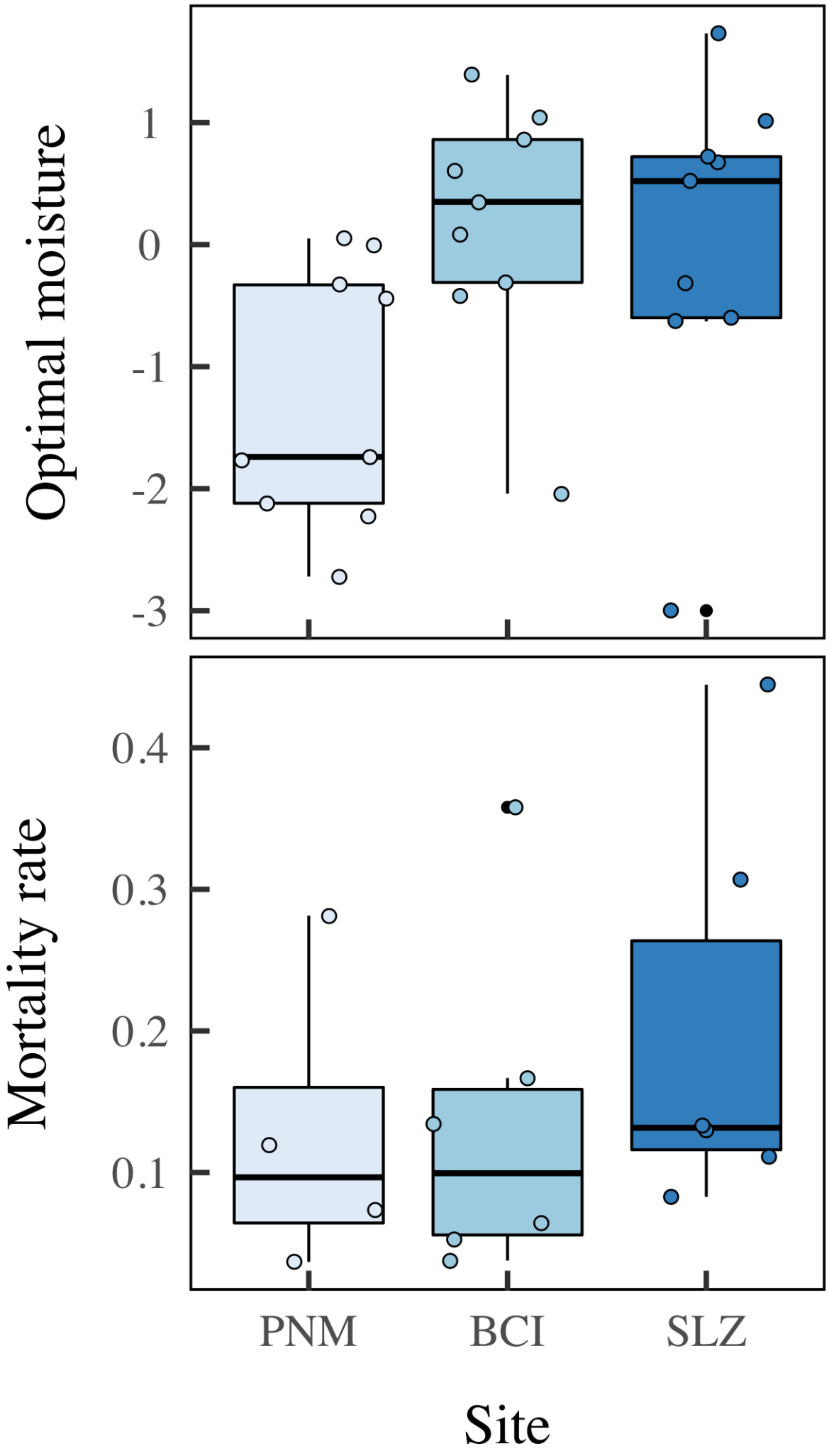
Optimal moisture
1
0
-1
-2
-3
Mortality rate
0.4
0.3
0.2
0.1
PNM
BCI
SLZ
Site

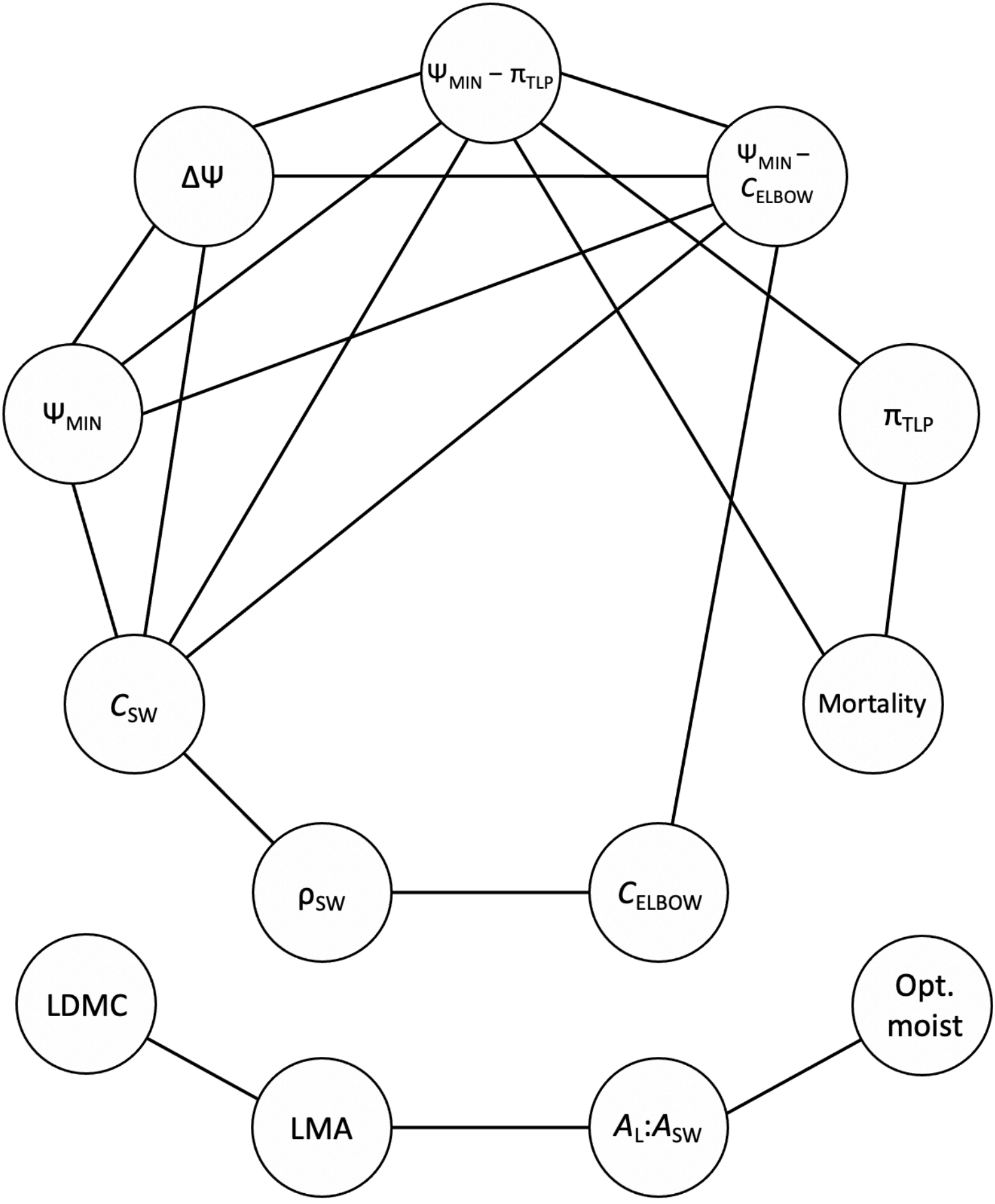
$\Psi_{MIN} - \pi_{TLP}$
$\Delta\Psi$
$\Psi_{MIN} - C_{ELBOW}$
Ψ_{MIN}
π_{TLP}
C_{SW}
Mortality
ρ_{SW}
C_{ELBOW}
LDMC
Opt. moist
LMA
$A_L:A_{SW}$

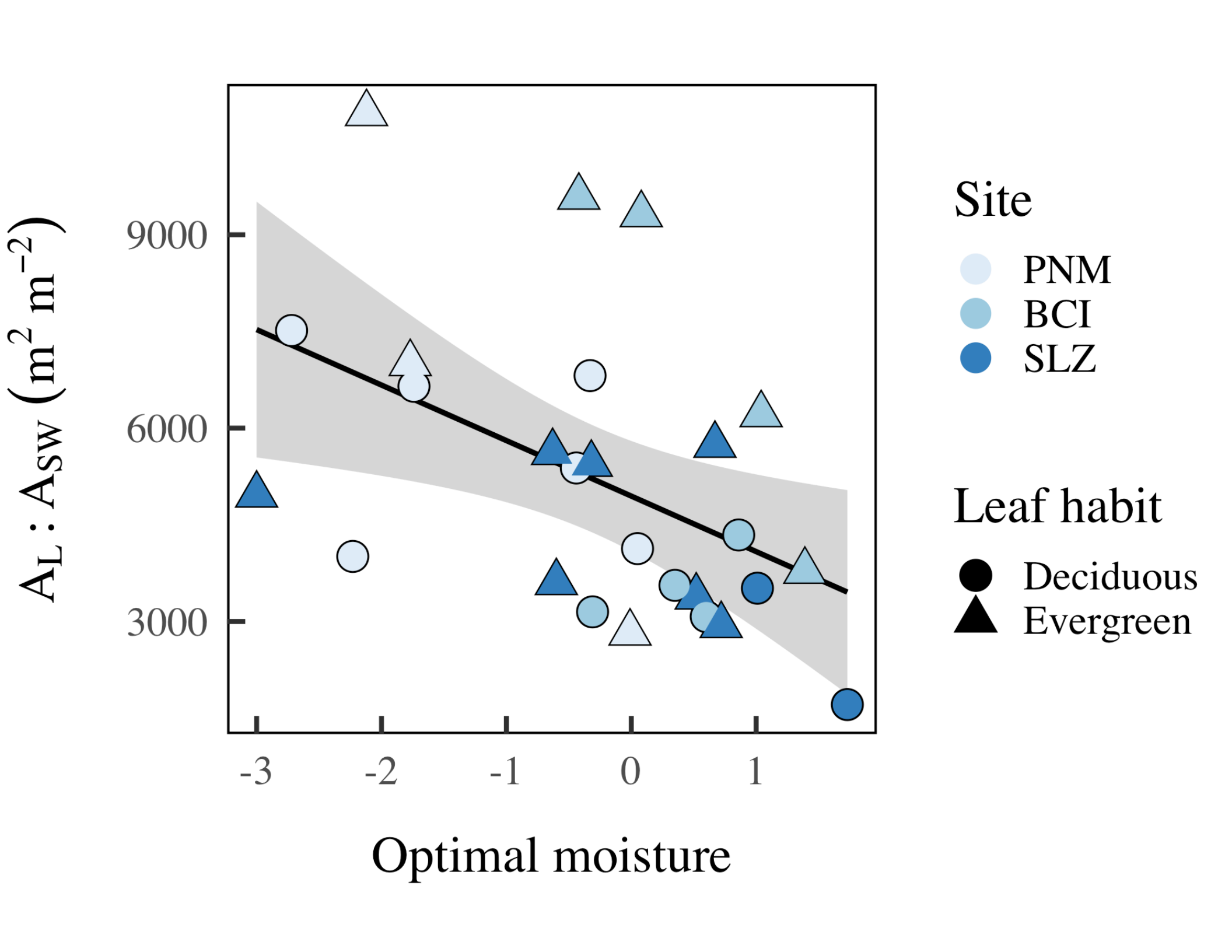
$A_L : A_{SW}$ (m^2 m^{-2})
9000
6000
3000
-3
-2
-1
0
1
Optimal moisture
Site
PNM
BCI
SLZ
Leaf habit
Deciduous
Evergreen